J. Fluid Mech. (1984), *vol.* 141, *pp.* 139–178
Printed in Great Britain

The mixing layer: deterministic models of a turbulent flow. Part 3. The effect of plane strain on the dynamics of streamwise vortices

By S. J. LIN
Scientific Research Associates, P.O. Box 498, Glastonbury, Connecticut 06033
AND G. M. CORCOS
University of California, Berkeley, CA 94270

(Received 11 May 1983 and in revised form 23 November 1983)

...in hydrodynamic turbulence... the fate of vortices extending in the direction of motion is of great importance (J. M. Burgers 1948).

We examine an elementary model of the dynamics of streamwise vorticity in a plane mixing layer. We assume that the vorticity is unidirectional and subjected to a two-dimensional spatially uniform strain, positive along the direction of vorticity. The equations of motion are solved numerically with initial conditions corresponding to a strain–viscous-diffusion balance for a layer with a sinusoidal variation of vorticity. The numerical results are interpreted physically and compared to those of an asymptotic analysis of the same problem by Neu. It is found that strained vortex sheets are fundamentally unstable unless their local strength nowhere exceeds a constant (somewhat larger than 2) times the square root of the product of strain and viscosity. The instability manifests itself by the spanwise redistribution of the vorticity towards the regions of maximum strength. This is accompanied by the local rotation of the layer and the intensification of the vorticity. The end result of this evolution is a set of discrete round vortices whose structure is well approximated by that of axially symmetric vortices in an axially symmetric strain. The phenomenon can proceed (possibly simultaneously) on two separate lengthscales and with two correspondingly different timescales. The first lengthscale is the initial spanwise extent of vorticity of a given sign. The second, relevant to initially thin and spanwise slowly varying vortex layers, is proportional to the layer thickness. The two types of vorticity focusing or collapse are studied separately. The effect of the first on the diffusion rate of a scalar across the layer is calculated. The second is examined in detail for a spanwise-uniform layer: First we solve the eigenvalue problem for infinitesimal perturbations and then use the eigenfunctions as initial conditions for a numerical finite-differences solution. We find that the initial instability is similar to that of unstrained layers, in that roll-up and pairings also follow. However, at each stage a strain–diffusion balance eventually imposes the same cross-sectional lengthscale and each of these events leads to an intensification of the local value of the vorticity.

The parameters upon which collapse and its timescale depend are related to those which are known to govern a mixing layer. The results suggest that the conditions for collapse of strained vortex sheets into concentrated round vortices are easily met in a mixing layer, even at low Reynolds numbers, so that these structures whose size is the Taylor microscale are far more plausibly typical than are vortex sheets on that

scale. We found that they raise significantly the diffusion rate of scalar attributes by enhancing the rate of growth of material surfaces across which diffusion takes place. Finally, experimental methods that rely on the visualization of the gradient of scalar concentration are shown to be unable to reveal the presence of streamwise vorticity unless that vorticity has already gathered into concentrated vortex tubes.

1. Introduction

In Part 2 (Corcos & Lin 1984) we have given an account of the origin of three-dimensional components of the motion in a free shear layer which develops in time, a T-layer. According to our model, a developing and pairing two-dimensional layer fosters the growth of initially small three-dimensional perturbations so that the vorticity whose initial dominant direction is spanwise acquires a component normal to the span, the 'streamwise' vorticity $\tilde{\omega}$. The spanwise component is also modified by the new motion. Nevertheless the important features of the two-dimensional flow studied in Part 1 (Corcos & Sherman 1984) survive. We discovered in particular how the characteristic patterns of strain and of spanwise vorticity of the base flow constrain the new motion. According to our model equations, while the spanwise vorticity of the base flow soon migrates into a row of distinct vortices separated by regions which are almost totally depleted of spanwise vorticity, $\tilde{\omega}$ is found in a continuous layer. Between primary spanwise vortices, this layer has a simple structure: $\tilde{\omega}$ lies along the layer and the circulation associated with it does not continue to increase with time. On the other hand, within the primary spanwise vortices, the streamwise vorticity layer is folded (several times during pairing), the direction of $\tilde{\omega}$ varies and a three-dimensional instability continues to feed it, though not monotonically in time.

In our model, the spanwise distribution of this vorticity was sinusoidal, with wavelength $\lambda_y = 2\pi/\beta$. This unrealistic feature is merely a consequence of the linearization of the model equation for the three-dimensional part $\boldsymbol{u}$ of the velocity vector $\boldsymbol{V} = \boldsymbol{U}+\boldsymbol{u}$, and of the chosen initial conditions. It is of course possible, as Riley & Metcalfe (1980), Cain, Reynolds & Ferziger (1981), Couët & Leonard (1980) and Brachet & Orszag (1982) have done, to carry out the numerical solution of a discrete approximation to the fully nonlinear three-dimensional problem. But we fear that the interpretation of the numerical results of such computations is made difficult by what amounts to the superposition of several different dynamical events. One of these is the instability that fuels the three-dimensional motion, the subject of Part 2; another is the evolution of the newly created vorticity in the presence of an imposed field of strain. The latter problem, which has received comparatively little attention, is quite complex in all its generality and can profitably be examined first by itself and in a context which is admittedly restrictive, but which allows sharper characterization. The goal is to comprehend new elementary prototypes of motion relevant to the mixing layer, as well as to other turbulent flows.

2. The model

Assume an initial unidirectional vorticity distribution

$$\boldsymbol{\omega} = \hat{\boldsymbol{e}}_x \omega_1(y, z)$$

subjected to a plane strain field

$$\boldsymbol{U} = \hat{\boldsymbol{e}}_x \gamma x - \hat{\boldsymbol{e}}_z \gamma z, \tag{2.1}$$

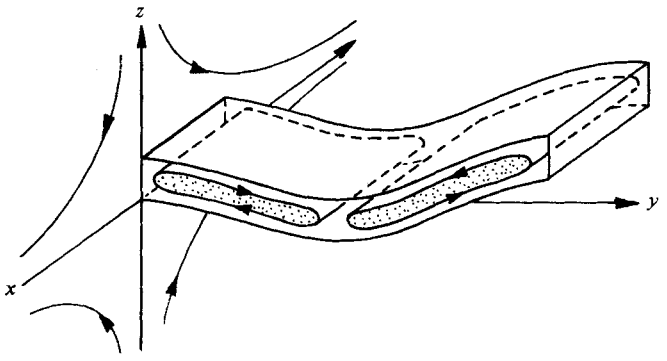

FIGURE 1. The model: unidirectional vorticity in a plane strain.

where $\hat{\boldsymbol{e}}_x$ and $\hat{\boldsymbol{e}}_z$ are unit vectors in the x- and z-directions and $\gamma(t)$ is a prescribed strain rate, which remains independent of x, y and z. This geometrically simple model sketched in figure 1 is a good approximation (see Part 2) to the local flow along the braids and provides the most elementary form of an interesting problem: what distribution of vorticity results when vortices are subjected to mutual and self-induction as well as to strain along their axes and to viscous diffusion? The model allows in particular solutions in which the velocity components v and w normal to the direction of the vorticity remain independent of x if they are so initially. Thus the continuity and momentum equations reduce to

$$\frac{\partial v}{\partial y}+\frac{\partial w}{\partial z}=-\gamma, \tag{2.2a}$$

$$\frac{\partial v}{\partial t}+v\frac{\partial v}{\partial y}+w\frac{\partial v}{\partial z}=-\frac{1}{\rho}\frac{\partial p}{\partial y}+\nu\left(\frac{\partial^2 v}{\partial y^2}+\frac{\partial^2 v}{\partial z^2}\right), \tag{2.2b}$$

$$\frac{\partial w}{\partial t}+v\frac{\partial w}{\partial y}+w\frac{\partial w}{\partial z}=-\frac{1}{\rho}\frac{\partial p}{\partial z}+\nu\left(\frac{\partial^2 w}{\partial y^2}+\frac{\partial^2 w}{\partial z^2}\right). \tag{2.2c}$$

The velocity vector is $\boldsymbol{V}=\hat{\boldsymbol{e}}_x\gamma x+\hat{\boldsymbol{e}}_y v+\hat{\boldsymbol{e}}_z w$. The asymptotic values of v and w are

$$v\to 0, \quad w\to -\gamma z \quad \text{for} \quad z\to\pm\infty.$$

An initially x-independent distribution of the passive scalar with asymptotic values,

$$\rho\to\mp\tfrac{1}{2}\Delta\rho \quad \text{as} \quad z\to\pm\infty,$$

will also remain x-independent and is governed by

$$\frac{\partial \rho}{\partial t}+v\frac{\partial \rho}{\partial y}+w\frac{\partial \rho}{\partial z}=D\left(\frac{\partial^2 \rho}{\partial y^2}+\frac{\partial^2 \rho}{\partial z^2}\right), \tag{2.2d}$$

where D is the molecular diffusivity coefficient for ρ.

The vorticity equation for our model flow is

$$\frac{\partial \omega_1}{\partial t}-\gamma\left(z\frac{\partial \omega_1}{\partial z}+\omega_1\right)-\nu\left(\frac{\partial^2 \omega_1}{\partial y^2}+\frac{\partial^2 \omega_1}{\partial z^2}\right)=-v\frac{\partial \omega_1}{\partial y}-\tilde{w}\frac{\partial \omega_1}{\partial z}, \tag{2.3}$$

where $w=\tilde{w}-\gamma z$. Its only known exact solution represents a vortex layer, uniform in the spanwise direction. It is therefore inappropriate for a shear layer across which the total circulation in any (y, z)-plane vanishes.

2.1. *Weak vortices*

Suppose that a row of weak alternating vortices is initially represented by

$$\omega_1 = \omega_0(z/\delta_1)\cos\beta y,$$

where ω_1 is negligible for $|z| > \delta_1$. If we define Γ as the circulation round one of the vortices along a rectangular circuit of sides $\frac{1}{2}\lambda_y = \pi/\beta$ and $2\delta_1$, we find that the right-hand terms of (2.3) are negligible compared with the strain-related transport and stretching terms on the left provided that

$$\Gamma^* \equiv \frac{\Gamma}{\gamma\lambda_y^2} \ll 1. \tag{2.4}$$

Thus if the inequality (2.4) is satisfied, the vorticity equation can be approximated by the linearized equation†

$$\frac{\partial\omega_1}{\partial t} - \gamma z\frac{\partial\omega_1}{\partial z} = \gamma\omega_1 + \nu\left(\frac{\partial^2\omega_1}{\partial y^2} + \frac{\partial^2\omega_1}{\partial z^2}\right). \tag{2.5}$$

Equation (2.5) has a similarity solution of the form

$$\omega_1 = \Omega_0(t)\,\omega(\eta)\cos\beta y, \tag{2.6a}$$

where $\eta = z/\delta(t)$, with boundary condition

$$\omega \to 0 \quad \text{as} \quad |\eta| \to \infty.$$

This solution is

$$\Omega_0(t) = \frac{\delta(0)\,\Omega_0(0)}{\delta(t)}\exp(-\beta^2\nu t), \tag{2.6b}$$

$$\delta^2 = \delta_0^2\exp\left(-\int_0^t 2\gamma(t')\,\mathrm{d}t'\right) + \pi\nu\int_0^t \exp\left(-\int_{t'}^t 2\gamma(t'')\,\mathrm{d}t''\right)\mathrm{d}t', \tag{2.6c}$$

and, provided that $\omega \to 0$ faster than $|\eta|^{-1}$ as $|\eta|$ becomes large,

$$\omega = \exp(-\tfrac{1}{4}\pi\eta^2). \tag{2.6d}$$

The circulation around a single vortex is given by

$$\Gamma = \pm 2\lambda_y\pi^{-1}\delta(0)\,\Omega_0(0)\exp(-\beta^2\nu t). \tag{2.6e}$$

Solution (2.6) describes a simple accommodation of streamwise vorticity to the competing effects of strain and diffusion.

(i) The circulation and the maximum vorticity both decay in a time of order $(\beta^2\nu)^{-1}$ as a result of spanwise diffusion of vorticity of alternating sign. This decay rate is slow in units of γ^{-1} if $\gamma/\beta^2\eta \gg 1$.

(ii) The thickness δ of the vorticity layer is the same as that found in Part 1 for the spanwise vorticity layer near stagnation points. There the rates of change of γ are such that δ frequently approaches its asymptotic value $\delta_a = (\pi\nu/2\gamma)^{\frac{1}{2}}$.

(iii) For a constant value of γ, the vortex aspect ratio reaches the asymptotic value

$$A_R = \frac{\lambda_y}{4\delta_a} = \left(\frac{1}{8\pi}\frac{\gamma\lambda_y^2}{\nu}\right)^{\frac{1}{2}} \tag{2.7}$$

† The argument leaves open the possibility that the small terms left out are destabilizing, i.e. that the solution of the complete vorticity equation departs progressively from that of (2.5). This is discussed in §4 and by Neu (1984*b*).

in a time of order $\gamma^{-1}[\delta^2(0)/\delta_a^2-1]^{\frac{1}{2}}$. If we identify γ as the strain created by the main spanwise vortices, say at the stagnation points, assign the typical value $3U/l$ (see Part 1) to this strain and further assume $\lambda_y \approx (\lambda_x)^0 \approx 15\delta_i$ as suggested by observation (Breidenthal 1981), where l is the spacing between spanwise vortices, $(\lambda_x)^0$ is the wavelength of the initial-layer two-dimensional instability and δ_i is the initial-layer thickness (which can be equated to $\delta(0)$ above),

$$A_R \approx 5.2(\delta_i/l)^{\frac{1}{2}}\, Re_i^{\frac{1}{2}},$$

where $Re_i = U\delta_i/\nu$ is the initial Reynolds number of the layer. For instance at the end of the first roll-up, $l = (\lambda_x)^0$ and

$$A_R \approx 1.5\, Re_i^{\frac{1}{2}}$$

According to our linearized solutions, the counter-rotating vortex cells are thus in general flattened and elongated along the span. But each time spanwise vortices pair, l doubles, γ is decreased by half and the aspect ratio decreases by the factor $2^{\frac{1}{2}}$.

The velocity components v and $\tilde{w}$ associated with the streamwise vorticity are evidently of the form

$$v = \Omega_0(t) f_2(t,z)\cos\beta y,$$

$$\tilde{w} = \Omega_0(t) f_3(t,z)\sin\beta y,$$

with

$$\frac{\partial v}{\partial y}+\frac{\partial \tilde{w}}{\partial z}=0, \quad \frac{\partial \tilde{w}}{\partial y}-\frac{\partial v}{\partial z}=\Omega_0\,\omega(\eta)\cos\beta y.$$

This leads to

$$v = F(t)\cos(\beta y)\,(G(z)-G(-z)), \tag{2.8a}$$

$$\tilde{w} = F(t)\sin(\beta y)\,(G(z)+G(-z)), \tag{2.8b}$$

where

$$F(t) = \tfrac{1}{2}\delta \exp\left(\frac{\beta^2\delta^2}{\pi}\right)\Omega_0(t) \tag{2.8c}$$

and

$$G(z) = \exp(\beta z)\,\mathrm{erfc}\left(\frac{\pi^{\frac{1}{2}}}{2\delta}z-\frac{\beta\delta}{\pi^{\frac{1}{2}}}\right). \tag{2.8d}$$

If the Reynolds number is such that $A_R \gg 1$, the velocity components v and $\tilde{w}$ decay slowly with z, i.e. on the scale of π/β outside the vorticity layer. In this case the vortices are essentially spanwise shear layers with a spanwise periodic variation of shear.

2.2. *The general case*

The solution above decays progressively while it remains self-similar. But the layer may in fact have an entirely different evolution. We ask the following questions.

(i) When $A_r \to \infty$, (2.6) tends to the exact solution of the full equations for an infinite strained vortex sheet. For large times this solution becomes stationary if γ is constant, but is it stable?

(ii) When A_R is finite, can the terms omitted in the linearization alter fundamentally the approximate balance between stretching and diffusion described by the similarity solution?

These two seemingly distinct questions are the two sides of the same coin. They both involve the evolution of vorticity strained both externally and by self-induction. We shall see that, for a sufficiently large aspect ratio and a sufficiently strong circulation, both departures from the similarity solution do occur side by side. But

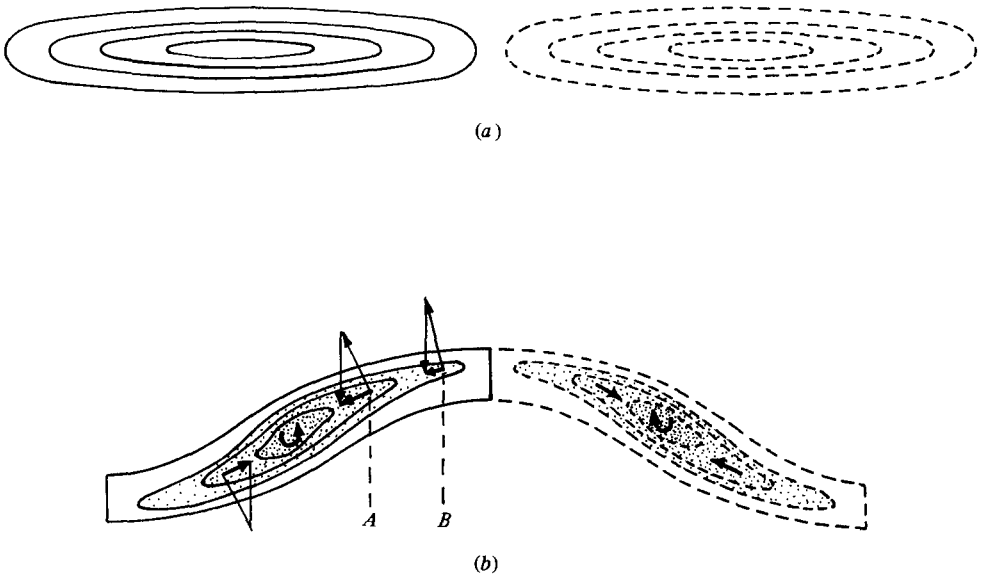

FIGURE 2. Sketch of the vorticity distribution: (*a*) according to the similarity solution (weak circulation); (*b*) showing the effect of strong circulation.

the time- and lengthscales that characterize these two types of evolution are different, so that, for computational as well as heuristic reasons, we shall examine them separately. Section 3 focuses on the large-scale features of the competition between external strain, diffusion and induction, while §4 examines the stability of the uniform-layer solution taken as a model of counter-rotating vortices of large aspect ratio. Section 5 discusses both in the context of the mixing layer.

3. The evolution of strained counter-rotating streamwise vortices

A sketch of a pair of stretched vortices of alternating circulation suggests how self-induction tends to modify the elementary solution of §2.1. Figure 2(*a*) shows contours of constant vorticity in the (y, z)-plane according to that solution. In figure 2(*b*), where the circulation is finite, the vortex centres remain on the plane $z = 0$, since by symmetry the velocity induced there by the vorticity of an infinite row vanishes. Elsewhere, the induced velocity tends to rotate the flattened vortices around the centres while the strain opposes this rotation with the vertical velocity $-\gamma z$. A balance would be possible were it not for the fact that the induced velocity has a component along the span y. Along the spine of the vorticity contours, at point A (near the centre of the vortex) that velocity should be approximately normal to the spine as it is for the Kirchhoff ellipse (see Lamb 1932 and §4.4), while at point B, i.e. close to a neighbouring vortex, it should be more nearly vertical. The sum of the induced velocity and of the z-component of the strain velocity is thus a vector directed approximately towards the vortex centre along the spine. Accordingly, in the absence of viscous diffusion, we might expect the vortices to become foreshortened.

3.1. *Numerical solutions*

We shall now illustrate the nonlinear evolution of counter-rotating vortices strained along their axes with finite-differences solutions of (2.2). These are first non-

dimensionalized by using λ_y as the lengthscale and γ^{-1} as the timescale. The pressure scale is $\rho_0 \lambda_y^2 \gamma^2$. Henceforth y and z are non-dimensional coordinates and τ is non-dimensional time. The subscript of λ_y is now omitted. In the absence of vorticity, the equations reduce to

$$v = 0, \quad w = -z.$$

The boundary conditions are

$$v \to 0, \quad w \to -z \quad \text{as} \quad z \to \pm\infty,$$

$$v(0,z) = v(1,z), \quad w(0,z) = w(1,z).$$

The initial conditions chosen are the asymptotic forms of the similarity solutions (2.6) with γ = constant. Thus

$$v(y,z,0) = E\cos 2\pi y\,[H(z,\tau) - H(-z,\tau)],$$

$$w(y,z,0) = E\sin 2\pi y\,[H(z,\tau) - H(-z,\tau)] - \gamma z,$$

where

$$E = \tfrac{1}{4}\pi\Gamma^* \exp 4\pi\delta^2, \quad H = \exp(2\pi z)\operatorname{erfc}\left(\frac{\pi^{\frac{1}{2}} z}{2\delta} + 2\pi^{\frac{1}{2}}\delta\right), \quad \delta = \left(\frac{\pi\nu}{2\gamma}\right)^{\frac{1}{2}}$$

and Γ^* is defined by (3.1).

Parameters

There are two parameters, the non-dimensional circulation

$$\Gamma^* = \Gamma/\gamma\lambda^2 \tag{3.1}$$

and the aspect ratio, i.e. the ratio of the spanwise spacing of the vortices to their initial thickness

$$A_{\mathrm{R}} = \frac{\lambda}{4\delta_{\mathrm{a}}} = (8\pi)^{-\frac{1}{2}}\left(\frac{\gamma\lambda^2}{\nu}\right)^{\frac{1}{2}}. \tag{3.2}$$

In most of the calculations γ is held constant, while in a few cases γ is varied in time so as to simulate the typical evolution of the strain at the stagnation point of a mixing layer as a result of successive pairings.

3.2. *The finite-differences scheme*

This scheme is an adaptation to the present problem of 'program KHINT', which was initially developed by Patnaik (Patnaik, Sherman & Corcos 1976), and then modified and fully documented by Sherman (1981). The computational domain is bounded by $0 \leqslant y \leqslant 1$ and by $-z_0 \leqslant z \leqslant z_0$, where $0.45 \leqslant z_0 \leqslant 0.90$. Mesh size for $y = \frac{1}{64}$ and for z varied from $2z_0/64$ to $2z_0/132$, depending on the estimated typical value of the vorticity-layer thickness.

3.3. *A few typical cases*

We start with a case for which $\Gamma^* = 0.08$ and $A_{\mathrm{R}} = 3.75$ (figure 3*a–c*). The two adjacent vortices of opposite circulation rotate rapidly until $\tau = \gamma t \approx 1$, when there is an approximate balance between the z component of the velocity induced by the vortices and the z-component $-\gamma z$ of the imposed strain velocity. During the same time, the value of vorticity decreases somewhat while the vortices first lengthen, and their thickness starts to increase. For the rest of the calculation ($1 < \tau \leqslant 3.0$) the vortices shorten and the vorticity decreases (although little at their centres). At the end of the run, the circulation has decreased to 0.83 times its initial value, while, according to the similarity solution (2.6), $\Gamma/\Gamma_0 = \exp(-\pi\tau/2A_{\mathrm{R}}) = 0.68$. Thus, while

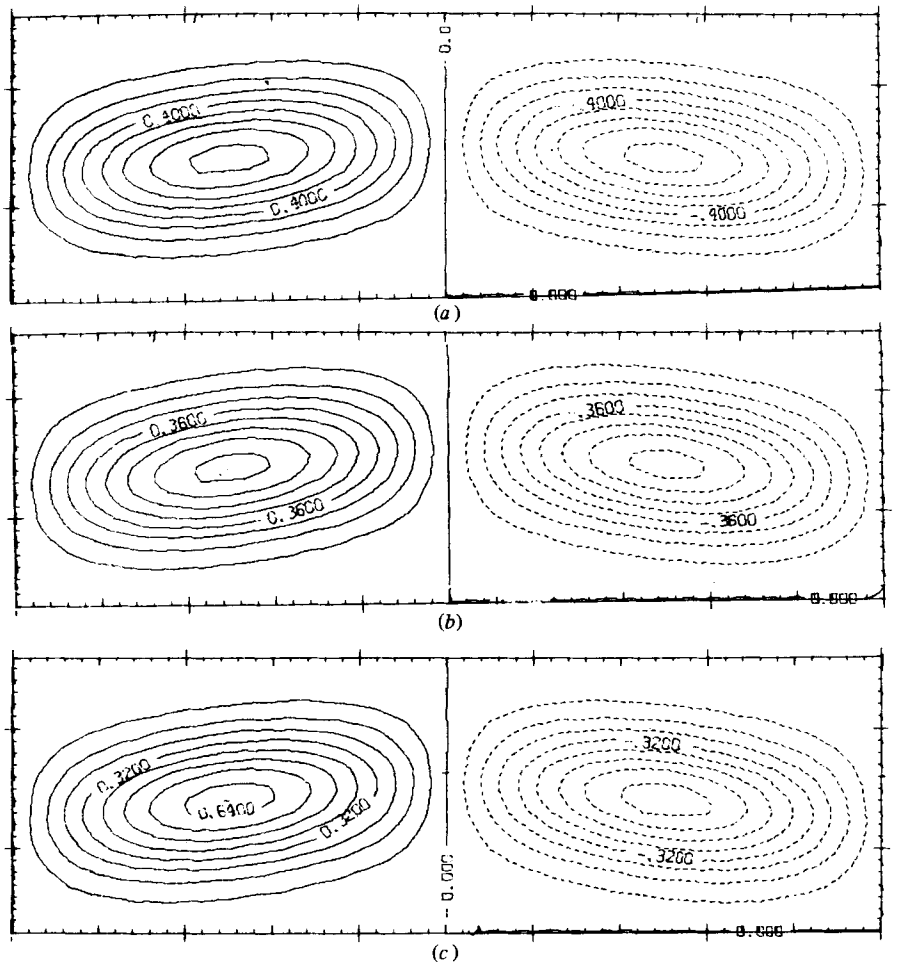

FIGURE 3. Vorticity contours: $\Gamma^* = 0.08$, $A_R = 3.75$; (*a*) $\tau = 1.0$; (*b*) 2.0; (*c*) 3.0.

the vortices interdiffuse as in the linear solution, diffusion is less effective here because the inward component of induced vorticity opposes this diffusive flux, especially near the centres of the vortices. Nevertheless, their evolution during the time of the calculation is qualitatively similar to that described in the linear solution. The evolution for later times can be surmised: Because the vortices gradually lose their circulation, their tilt with respect to the x-axis decreases. This trend is already

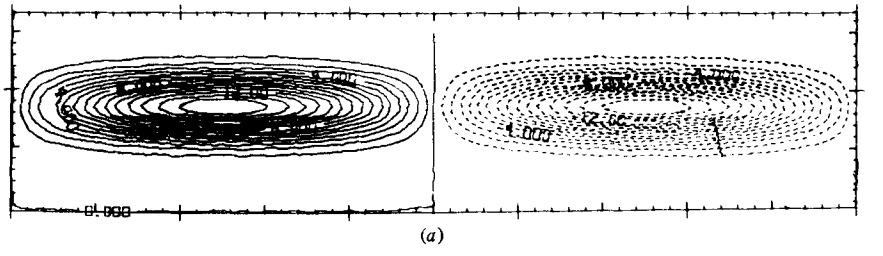

FIGURE 4. Vorticity contours: $\Gamma^* = 0.32$, $A_R = 7.95$: (*a*) $\tau = 0$; (*b*) 0.5; (*c*) 1.0; (*d*) 1.5.

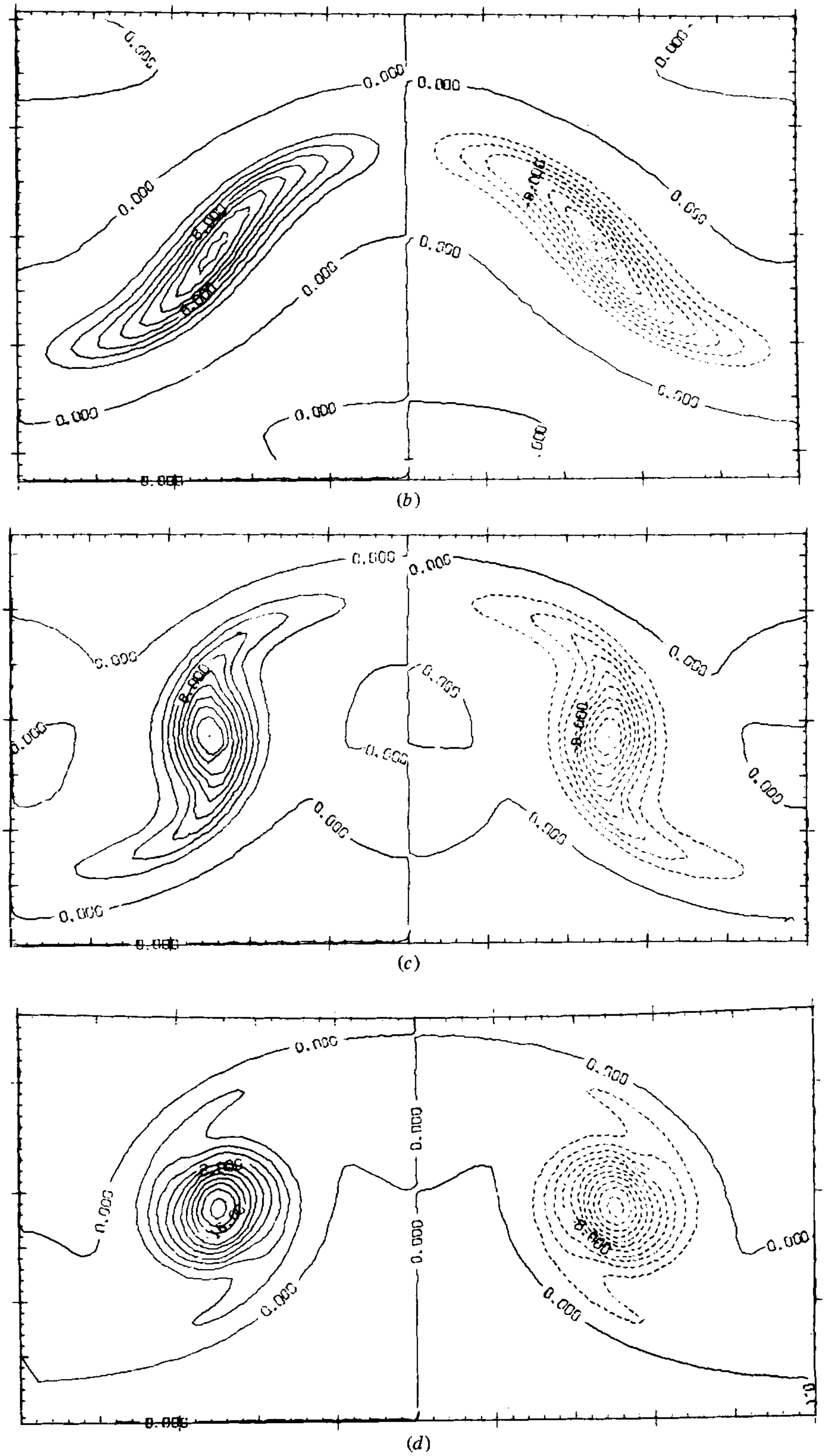

FIGURE 4 (*b*–*d*). For caption see facing page.

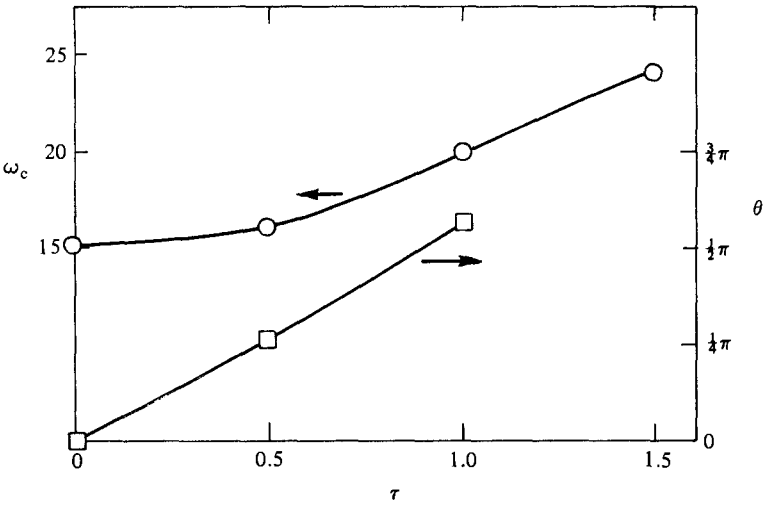

FIGURE 5. ○, vorticity at the vortex centres; □, tilt angles of vortices near centre as functions of time. $\Gamma^* = 0.32$, $A_R = 7.95$.

noticeable at $\tau = 3.5$. As a result, the advective flux of vorticity towards the vortex centres decreases, the vortex length increases again as a result of diffusion, and the vorticity distribution approaches asymptotically that of the initial state as it continues to decay.

Thus, for the case above (thick vortices, weak circulation), the effect of self-induction amounts only to a temporary and mild departure from the evolution given by the similarity solution.

A different history is apparent if the viscosity is decreased by a factor of about 4 and the circulation is increased by 4. This is shown on figure 4(*a*, *d*), where $A_R = 7.95$, $\Gamma^* = 0.32$. First, the thinner vortices bend noticeably as they tilt in that the tilt angle is larger near the vortex centres than towards the tips. Then it seems as though the central part of the vortices and the tips have a different, indeed, an opposite evolution: the central part swells, shortens and rotates steadily (fig. 5) while the tips thin out, elongate and lose their tilt. The value of the vorticity rises at the centre and at $\tau = 1.5$ the vortex is almost round, except for the remnants of its tip, which appear to rotate with the vortices and which are about to disappear. The end state in this case can also be plausibly imagined.

Since the vortices are now more concentrated and have lost only a small fraction of their circulation (figure 6), they will rotate and shrink until radial diffusion balances the *average* inward advection due to the strain. Induction due to the pair of neighbouring vortices and the rest of the row will be ineffective because the ratio of vortex radius to vortex spacing is now small. For the same reason, spanwise diffusion will be greatly decreased. More specific details of the asymptotic state are given in §3.5.

Departures from the similarity solution are entirely due to the vorticity-induced advection. If only diffusion is able to combat the focusing effect of that advection, collapse of the vortices should result for a given value of A_R for sufficiently large values of Γ^*, and equally, with a given value of Γ^*, for sufficiently large values of A_R. However, collapse will look different as A_R is varied: since the asymptotic radius of the collapsed vortex should be of the order of its initial thickness (see §3.5), the

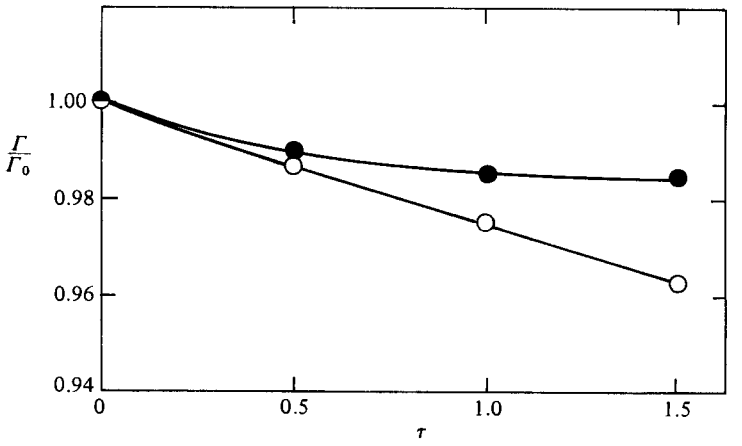

FIGURE 6. The decay of circulation with time: ○, according to the similarity solution; ●, according to the numerical solutions. $\Gamma^* = 0.32$, $A_R = 7.95$.

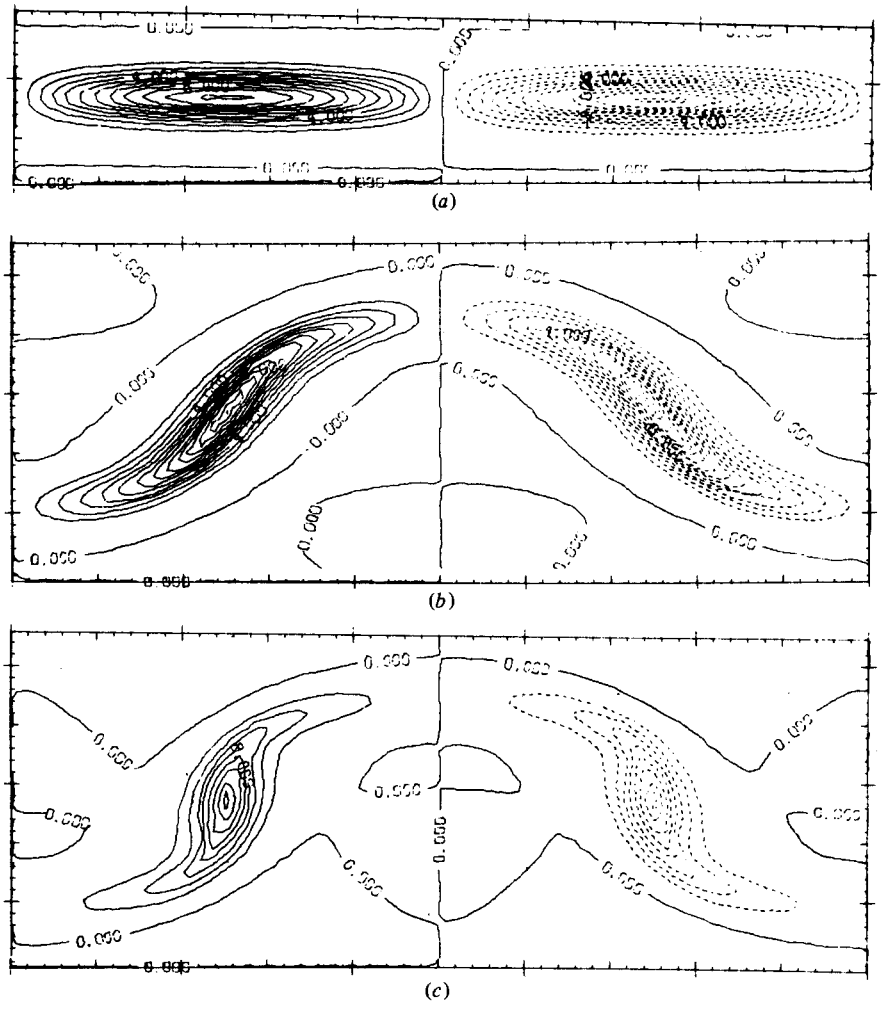

FIGURE 7. Vorticity contours: (*a*) $\tau = 0$; (*b*) 1.0; (*c*) 1.5. $\Gamma^* = 0.16$, $A_R = 11.25$.

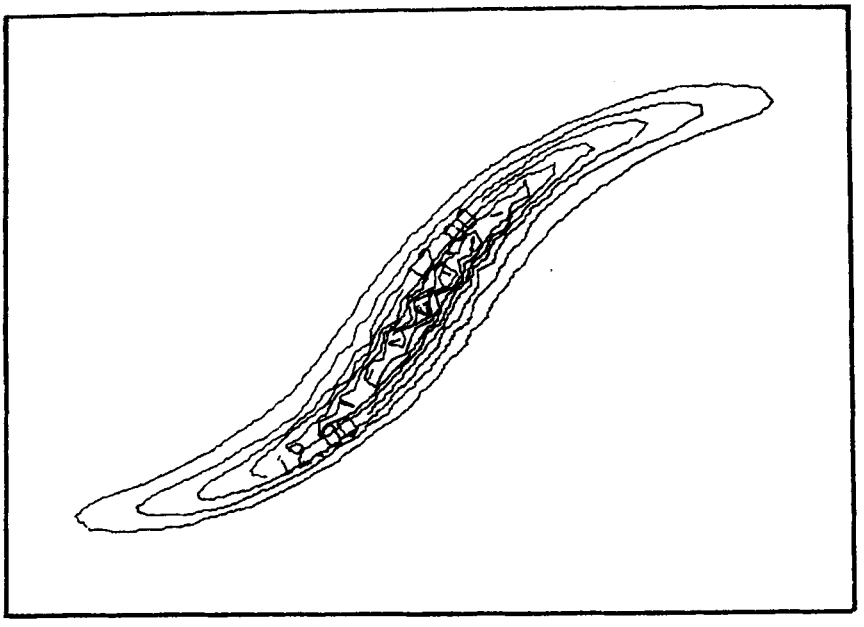

FIGURE 8. Vorticity contours for an elongated vortex in which shear instability develops prior to collapse. $\Gamma^* = 0.24$, $A_R = 18$, $\tau = 1.01$.

extent of the transformation from the initial to the end state, i.e. the ratio of initial to final vortex area and of final to initial value of maximum vorticity should vary directly with A_R.

Figure 7 (*a–c*) for the case $A_R = 11.25$, $\Gamma^* = 0.16$ illustrate the suggestion made above that collapse (impending in figure 7*c*) can be achieved with a smaller value of Γ^* provided the value of A_R is increased. Figure 7 (*b*) also suggests that the central part of the vortex may be subject to a wavy short-scale oscillation, which disappears (figure 7*c*) when the core becomes less elongated. This new scale of motion is prominent before collapse in cases for which A_R is even larger (figure 8). In such cases, the mesh size of the finite-difference grid is not fine enough to resolve the motion with satisfactory accuracy. But we varied mesh size, hand-plotted the vorticity contours directly from the numerical output, estimated wavelength and growth rates from the results of §4.1 (which considers this type of instability in much greater detail), and noted that the motion is damped out later by the collapse of the layer. All this convinces us that these minute features of the dynamic evolution are not due to numerical instability of the computation or of the graphical display technique. They seem be be genuine evidence of the instability of the strained vortex layer to perturbations scaled on its thickness: we encounter here side by side the two types of dynamical events that were queried in §2.2. Section 4 considers this instability more accurately and in greater detail.

3.4. *Scaling: a heuristic model*

When Γ^* is small, the vortices appear to stop rotating around their centres before the end of the calculation. But their subsequent evolution is sometimes in doubt because it seems to follow a different, slower, timescale. We now use physical

arguments and a simple model to gain an idea of the times required for tilting and for collapsing the vortices, and we derive heuristically a collapse condition.

We idealize the evolution of the weak or moderately strong vortices by assuming that they rotate on a timescale τ_e which is smaller than the timescale for collapse τ_c, and that for $\tau \leqslant \tau_e$, their initial tilt or equilibrium angle θ_e is moderately small (e.g. $\frac{1}{6}\pi$).

3.4.1. *Rotation time*

τ_e is the value of τ at which the velocity of the vortices normal to their length and due to self-induction temporarily balances the component of the strain velocity in the same direction, i.e.

$$\dot{\theta} = \tfrac{1}{2}\gamma \sin 2\theta_e. \tag{3.3}$$

Here $\dot{\theta}_0$ is the initial angular velocity of a vortex and θ_e is the equilibrium angle. The rotation time $\tau_e = \int_0^{\theta_e} \dot{\theta}^{-1}\, d\theta$ is crudely evaluated from the average of the initial value θ_0 and the end value $\theta = 0$, which yields

$$\tau_e = t_e \gamma \approx 2. \tag{3.4}$$

The main point is that, if a temporary approximate balance exists between strain and self-induction, the time needed to reach it depends only weakly on the circulation.

3.4.2. *Inviscid collapse time*

τ_c is obtained as follows. We use, as a model for our vortices, the elliptic vortex of uniform vorticity discussed by Kirchhoff (e.g. Lamb 1932). The major axis is assumed initially coincident with the y-axis. In the absence of imposed strain, such a vortex has a uniform rotation rate

$$\dot{\theta}_0 = \frac{\Gamma}{\pi(a+b)^2}, \tag{3.5}$$

where Γ is its circulation, and a and b are the semimajor and semiminor axes. Thus (3.3) becomes approximately for an elongated ellipse†

$$\sin 2\theta_e = \frac{2\Gamma}{\pi(a+b)^2\gamma}. \tag{3.6}$$

Along the major axis, the unbalanced velocity component in the direction of the vortex centre is (figure 2*b*)

$$v_s = \dot{\theta}_0 s \tan\theta_e,$$

or, according to (3.5) and (3.6),

$$v_s = \frac{\Gamma^2 s}{\gamma\pi^2(a+b)^4\cos^2\theta_e}, \tag{3.7}$$

and the non-dimensional collapse time is

$$\gamma t_c = \tau_c = \frac{a\gamma}{v_s}\pi^2\cos^2\theta(1+\eta)^4\frac{\gamma^2 a^4}{\Gamma^2},$$

† For an exact solution of the problem of the uniformly strained Kirchoff vortex see Neu (1984*a*).

where $\eta = b/a$. If we identify a with $\frac{1}{4}\lambda$,

$$\tau_c \approx 0.04(1+\eta)^4 \cos^2\theta\, \Gamma^{*-2} \tag{3.8}$$

For small values of Γ^*, $\tau_c \gg \tau_e$, the collapse time increases inversely with the square of the circulation, and according to our model it increases with the thickness of the vortex. We have somewhat underestimated the value of τ_c since

(i) the effect of the rest of the row of vortices is such as to decrease the value of v_s, especially near the vortex tips;

(ii) we have not taken viscous diffusion into account.

3.4.3. *A collapse criterion*

Locally, viscous diffusion tends to transport vorticity away from the vortex centres while induction tends to advect it towards these centres. A local collapse criterion is obtained by equating the two transport rates. According to the self-similar solution with

$$\sigma(y) = \int_{-\infty}^{\infty} \omega\, dz,$$

$$\sigma = \sigma_0(0)\cos(\beta y)\exp(-\beta^2 \nu t),$$

where $\sigma_0(0)$ is the vortex strength at $y = 0$ and $t = 0$. Hence

$$\frac{\partial \sigma}{\partial t} = \nu \frac{\partial^2 \sigma}{\partial y^2},$$

and the viscous flux of strength σ is simply $\nu\, \partial\sigma/\partial y$. For our tilted vortex of finite strength, a local diffusion–advection balance requires approximately

$$\nu \frac{\partial \sigma}{\partial s} + \sigma v_s = 0, \tag{3.9}$$

where s is the direction of the vortex major axis and v_s, the component of velocity along this axis and towards the vortex centre. If we use the Kirchoff vortex whose strength is

$$\sigma = \sigma_0 \left[1 - \left(\frac{s}{a}\right)^2\right]^{\frac{1}{2}},$$

and the expression (3.7) for v_s, we find that (3.9) leads to

$$\frac{\sigma}{2(\gamma\nu)^{\frac{1}{2}}} \frac{1}{(1+\eta)^2 \cos\theta_e} = 1. \tag{3.10}$$

Now

$$\frac{\sigma}{2(\gamma\nu)^{\frac{1}{2}}} = 2^{\frac{1}{2}}\pi^{\frac{3}{2}} \Gamma^* A_R \frac{\sigma(s)}{\sigma_0}.$$

Thus our local collapse criterion gives the minimum value σ_c of σ for collapse as

$$\frac{\sigma_c}{\sigma_0} \frac{\Gamma^* A_R}{\cos\theta_e} \frac{1}{(1+\eta)^2} \approx 0.13. \tag{3.11}$$

In particular, for very elongated initial vortices ($A_R \gg 1$), (3.11) implies that the value of Γ^* required for collapse is quite small, and according to (3.6), $\theta \approx (2^4/\pi)\Gamma^*$ is also small, so that for this limiting case the collapsing criterion becomes

$$\frac{\sigma}{2(\gamma\nu)^{\frac{1}{2}}} = 1 \quad \text{or} \quad \Gamma^* A_R \frac{\sigma_c}{\sigma_0} \approx 0.13. \tag{3.12}$$

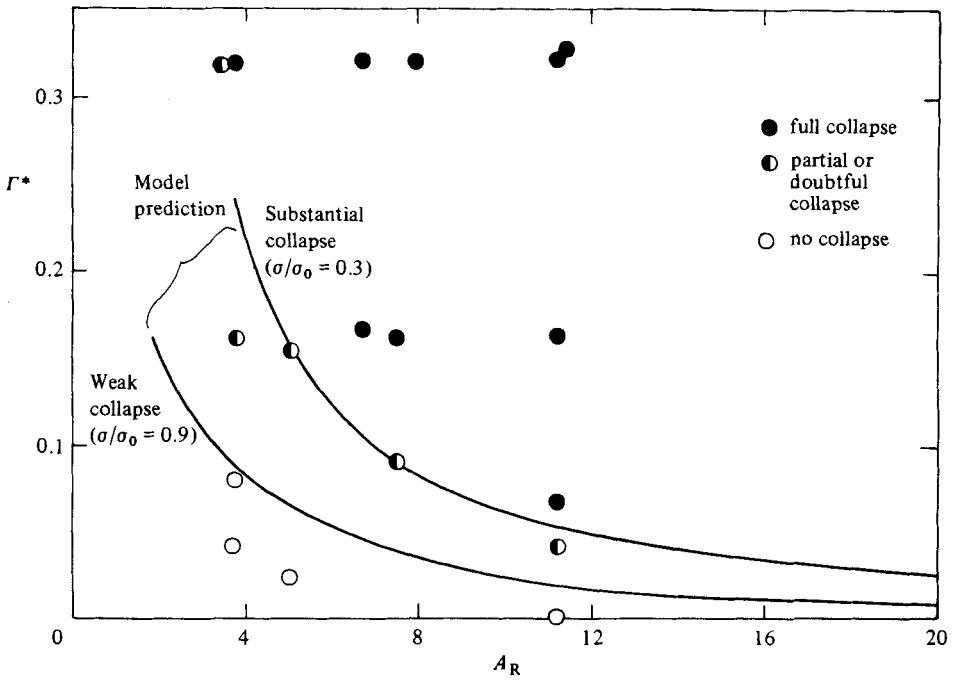

FIGURE 9. The collapse predictions of a simple model and the results of the numerical solutions.

Thus, if $\Gamma^* A_R < 0.13$, according to our simple model, diffusion of vorticity dominates concentration by induction and the strength decreases everywhere along the vortex, while, if $A_R > 0.13$, only the outer part of the vortex (that for which $\sigma/\sigma_0 < 0.13(\Gamma^* A_R)^{-1}$ is diffused, while the rest is driven inwards, continues to rotate, gains in strength and collapses.

Neu (1984*b*) offers an asymptotic analysis which applies precisely to the case $\Gamma^* \ll 1$, $A_R \gg 1$ and which yields (3.12) for an arbitrary initial distribution $\sigma(y)$.

For finite aspect ratios, (3.11), whose accuracy for a single elliptic strength distribution is $O(\eta)$ only, and which is not properly applicable to other distributions, may nevertheless be adapted to our case for which $\sigma = \sigma_0 \cos(2\pi x/\lambda)$ by evaluating for one case an effective b/a from the constant-vorticity contours and assigning a value of a/λ which yields the tilt angle θ_e found in the calculations. We can then compare and complement the results of the numerical solutions with model expectations. This is helpful because the limiting case envisaged in (3.12) is not approachable by our numerical solutions for two reasons:

(i) the thickness of the layer is so small as to require an excessively fine mesh;

(ii) the collapse time is so long that computation expenses are prohibitive. The opposite case is easily resolved in a reasonable computing time, but, as was already remarked, it is also less interesting since it offers no sharp boundary between a collapsing and a non-collapsing case because the vortex width is initially only somewhat larger than its thickness. On figure 9 two solid lines are shown. These are heuristic model predictions for collapse of two fixed fractions of our vortices: for points on the upper line, the fraction of the vortices with $\sigma/\sigma_0 > 0.3$ should collapse. On the lower line only the fraction of the vortex for which $\sigma/\sigma_0 > 0.9$ should collapse. Essentially, then, pairs of values of Γ^* and A_R that lie above the upper line yield

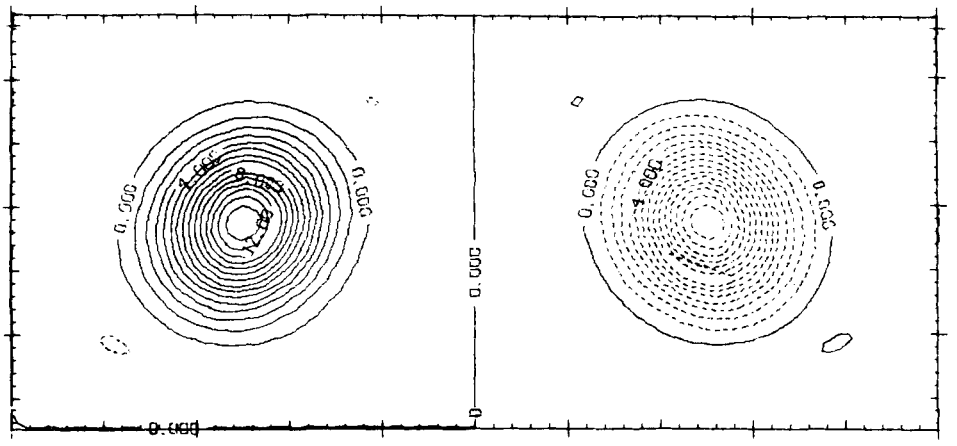

FIGURE 10. The vorticity contours are approaching the axially symmetric asymptotic state. $\Gamma^* = 0.64$, $A_R = 4.75$, $\Gamma/\nu = 360$, $\tau = 3.0$.

almost complete collapse, pairs that lie below the lower line are cases for which collapse does not occur, and pairs in between correspond to partial collapse. The filled circles characterize numerical solutions for which substantial collapse was either almost complete or well started at the end of the computation. The open circles denote cases in which decay was unambiguous, and the partially filled circles represent cases in which collapse was either partial or in doubt. We note that the model predictions are consistent with the results of the numerical solutions. The latter also bear out qualitatively the model result that the collapse time increases rapidly as Γ^* decreases.

3.5. *The asymptotic state after collapse*

Figure 10 shows the vorticity contours at $\tau = 3.0$ when $A_R = 4.73$ and $\Gamma^* = 0.64$. This is a case for which $\tau_c < \tau_e$, so that collapse is almost complete at $\tau = 3.0$. The contours are, perhaps surprisingly, very nearly circular even though the radius of the vortex is not small (about $\frac{1}{8}\lambda$). Apparently, the spinning vortex only senses a polar average of the strain.

Neu (1984*b*) has provided another asymptotic analysis for the last stages of the collapse in a plane strain by expanding the solution for a single vortex in powers of Γ/ν. The analysis shows that the leading term is the time-dependent axially symmetric solution for an axially symmetric strain first discussed by Burgers (1948):

$$\omega = \frac{\Gamma}{8\delta^2}\exp\left(-\frac{\pi r^2}{8\delta^2}\right), \tag{3.13a}$$

$$\delta^2 = \frac{\pi\nu}{2\gamma} + \left(\delta_0^2 - \frac{\pi\nu}{2\gamma}\right)\exp(-\gamma t), \tag{3.13b}$$

where γ is the (constant) axial strain rate. The first-order correction is $O(\nu/\Gamma)$. Accordingly, the effective inward strain is in fact the polar average of the plane strain, i.e. $\frac{1}{2}\gamma$.

Note that, in our notation, $\Gamma/\nu = 2^3\pi A_R^2\,\Gamma^* > 3.3A_R$, so that, if strained vortices collapse, $\Gamma/\nu \gg 1$. The effect of the rest of the vortex row which is not taken into account in Neu's analysis is to impose a strain γ_v in the (y,z)-plane which can be evaluated approximately as

$$|\gamma_v| \approx \pi\Gamma/\lambda^2.$$

Then the ratio of the two strains is

$$|\gamma_v/\gamma| \approx \pi\Gamma^*,$$

which is less than unity except for very strong vortices. Thus this second source of strain, which has a periodic distribution with zero average over a revolution of the vortex, is too weak to alter appreciably the asymptotic vorticity distribution which should be described accurately by (3.13).

This means that the intensification of the vorticity by the collapse and the corresponding decrease in the cross-sectional area of the vorticity can easily be given. For the initial state, $\Gamma_i = 2\pi^{-1}\lambda\delta\omega_0$, while for the final state $\Gamma_f = 8\delta^2\omega_0$, where ω_0 is the vorticity at the centre of the vortices in both cases. Thus the ratio r_ω of maximum vorticity after collapse $(\omega_0)_f$ to that before $(\omega_0)_i$ is

$$r_\omega = \frac{(\omega_0)_f}{(\omega_0)_i} = \frac{A_R}{\pi}\frac{\Gamma_f}{\Gamma_i}, \tag{3.14a}$$

where A_R is given by (2.7). For our assumed initial vorticity distribution the fraction γ_f/Γ_i of the total circulation which participates in the collapse is

$$\frac{\Gamma_f}{\Gamma_i} = \sin\frac{2\pi y_c}{\lambda},$$

where, at $y = y_c$, $\sigma = \sigma_c$, the value of σ given by (3.11). In practice (see e.g. §5.1 and figure 22), little vorticity escapes collapse by diffusion, so that Γ_f/Γ_i differs little from unity. Thus the vorticity amplification ratio is approximately

$$r_\omega \approx \left(\frac{\gamma\lambda_y^2}{8\pi^3}\right)^{\frac{1}{2}}.$$

If we use the typical values $\gamma \approx 3U/l$ (Part 1) and $\lambda_y \approx \lambda_{x_0} \approx 15\delta_i$ (Part 2 and Bernal 1981) then

$$r_\omega \approx 0.4\left(\frac{U\delta_i}{\nu}\right)^{\frac{1}{2}}. \tag{3.14b}$$

3.6. *The effect of streamwise vorticity on the diffusion of a scalar*

We now discuss the manner in which streamwise vorticity affects the diffusion of a scalar. The discussion can readily be extended to the study of chemical reactions for which reaction rates are sufficiently fast to be controlled by diffusion.

We assume that a passive scalar ρ with fixed diffusivity D has a uniform concentration far above the (x, y)-plane and a different uniform concentration far below it. The velocity is described by (2.2*a–c*), while the difference ρ between the scalar concentration and some fixed value ρ_0 obeys (2.2*d*) together with the boundary conditions

$$\rho(z) \to \mp\tfrac{1}{2}\Delta\rho \quad \text{as} \quad z \to \pm\infty.$$

Plane strain alone, i.e. the velocity $u = \gamma x$, $w = -\gamma z$, causes a transition layer to be created. Its thickness δ_0 is obtained from (2.6*c*) by replacing ν by D. This thickness is asymptotically constant for constant γ, i.e.

$$\delta_D = \left(\frac{\pi D}{2\gamma}\right)^{\frac{1}{2}}, \tag{3.15a}$$

while the concentration profile is given by

$$\rho = \tfrac{1}{2}\Delta\rho\,\mathrm{erf}\,[(\tfrac{1}{2}\pi)^{\frac{1}{2}}\eta], \tag{3.15b}$$

where $\eta = z/\delta_D$. In Part 1 we defined the mixed volume V_m, which in the context of our flow model is

$$V_m = \int_0^L \left[\iint_{\rho>0} \left(1 - \frac{2\rho}{\Delta\rho}\right) dy\, dz + \iint_{\rho<0} \left(1 + \frac{2\rho}{\Delta\rho}\right) dy\, dz \right] dx, \tag{3.16}$$

and showed that in two-dimensional flow

$$\frac{dV_m}{dt} = -2D \int_{\rho=0} \nabla\left(\frac{2\rho}{\Delta\rho}\right) \cdot \boldsymbol{n}\, ds.$$

Thus the rate of increase of mixed volume is twice the integral along the contour of zero concentration of the flux of normalized concentration across it.

The extension to our three-dimensional case for which ρ is independent of x is

$$\frac{dV_m}{dt} = 2D\, L(t) \int_{\rho=0} \delta_D^{-1}\, ds,$$

where $\delta_D = \Delta\rho/2(\partial\rho/\partial n)_{\rho=0}$. The volume considered has length $L(t)$ in the x-direction. Substituting (3.15a), we find that asymptotically, for a constant value of γ and for a volume of unit span and initial length L_0, the rate of increase of the mixed volume is, if the layer is only subjected to strain:

$$\frac{dV_m}{dt} = 2D\, \delta_D^{-1}\, L_0 \exp(\gamma t). \tag{3.17}$$

3.6.1. *Streamwise vorticity with weak circulation*

When streamwise vorticity is present, but (2.5) is applicable, the corresponding equation for ρ, to the same order of the small parameter, is simply

$$\frac{\partial\rho}{\partial t} - \gamma z \frac{\partial\rho}{\partial z} = D \frac{\partial^2\rho}{\partial z^2},$$

with solution (3.15), so that very weak vortices have no effect on the concentration. We have seen that, as long as the product $\Gamma^* A_R$ remains below a critical value, the vorticity pattern is not fundamentally altered, although it is rotated alternately clockwise and counter-clockwise by finite values of Γ^*. One may wonder under what circumstances the associated circulation is able to wind material surfaces around so that, in particular, for high values of $S_c \equiv \nu/D$, the thin diffusion layer might finally occupy the same volume as the vorticity, i.e. acquire a thickness comparable to δ. This question has been considered by H. King in work unpublished so far. It is difficult to treat it exactly for an unsteady velocity field. But we note that the decay indicated by (2.6) is typically slow since the characteristic decay time in units of γt is $\gamma\lambda_y^2/4\pi^2\nu \approx U\delta/\nu$ if $\gamma \approx 3U/\lambda_y$. Thus a quasi-steady approximation appears sufficient. Furthermore, it can be shown that the decay tends to decrease the rate at which a material surface is wound around. Now King finds that, for a steady flow,

---

FIGURE 11. The projection of particle trajectories onto the (y, z)-plane. Dots are particles originating on top and bottom boundaries at equal time intervals. After a sufficient time, the projection of particles originally on the horizontal material interface $z = 0$ lie on an asymptote shown as a solid curve. In case (a) (weak circulation), $z(y)$ is single-valued on that curve and there is only one diffusion layer across it. In case (b), a single Burgers vortex, $z(y)$ is multivalued on the asymptotic curve, diffusive layers are stacked around each other and overlap in the centre. The increased diffusion rate is primarily related to the resulting increase in the length of the material interface.

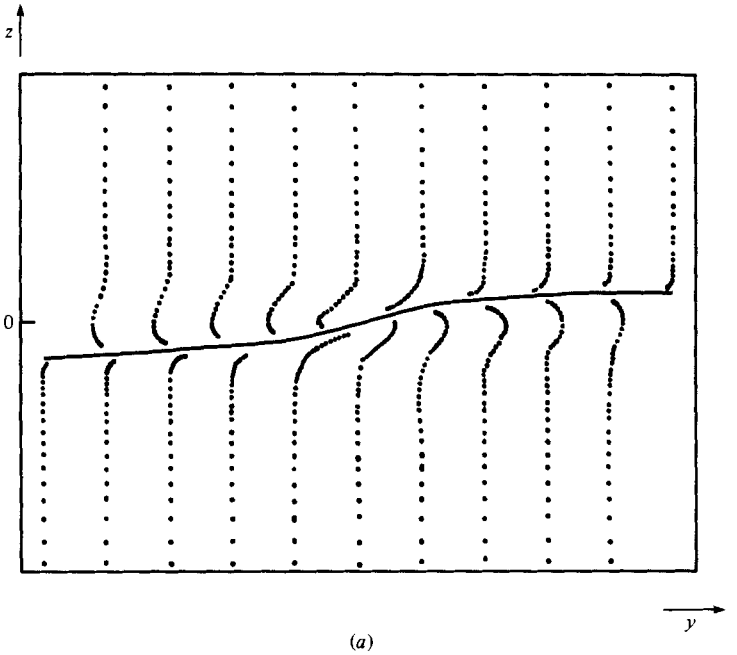

(*a*)

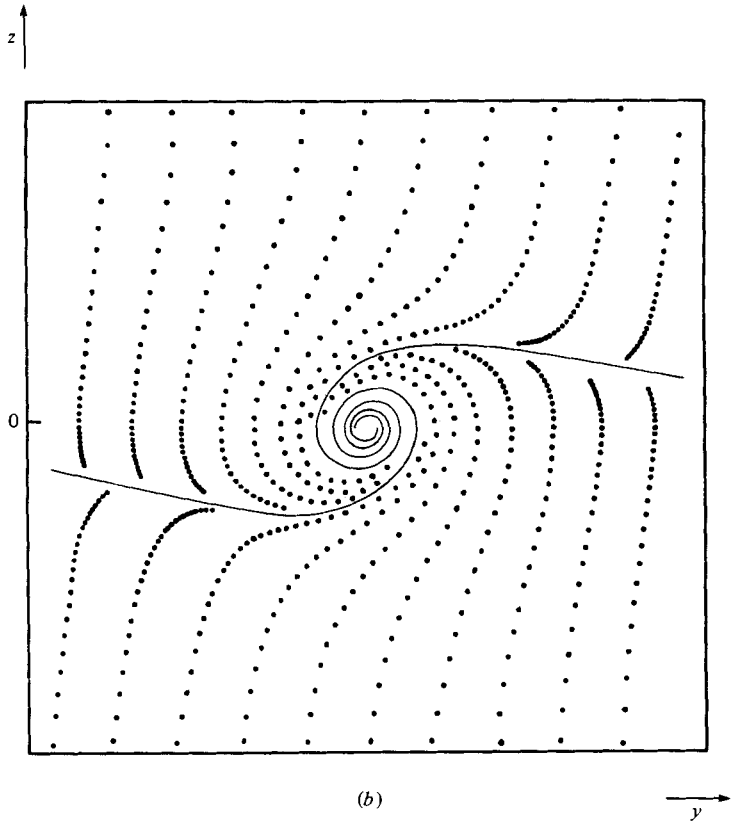

(*b*)

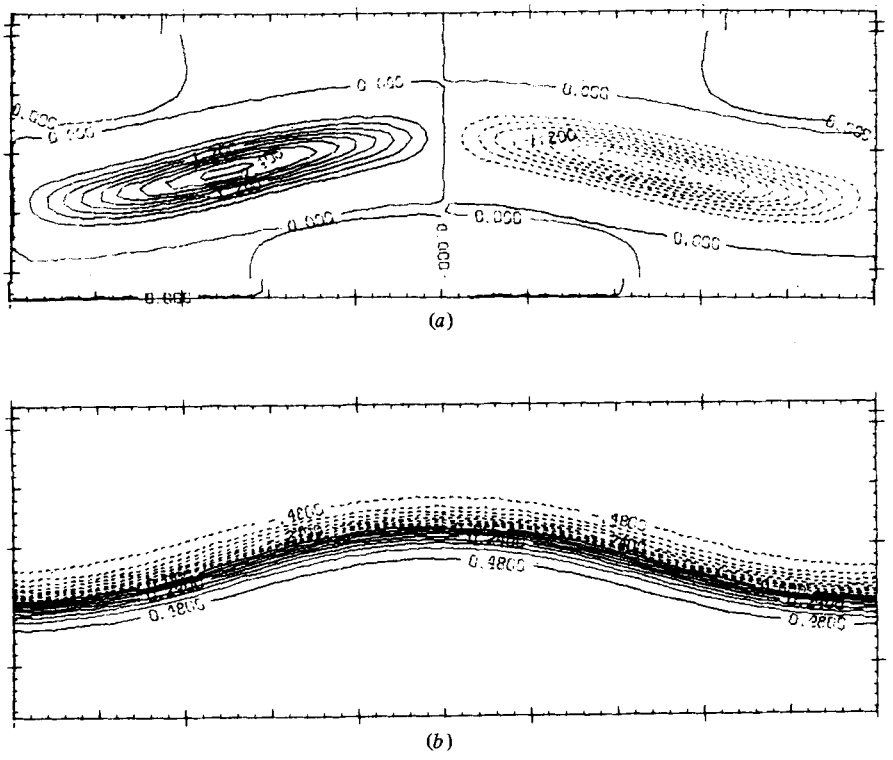

FIGURE 12. (a) Vorticity contours; (b) concentration contours. $\Gamma^* = 0.04$, $A_R = 11.25$, $\tau = 1.5$.

one of the necessary conditions for the roll-up of an initially plane material surface on which is found a stationary point of the induced velocity is that in some neighbourhood of this point the projection of particle trajectories onto the (y, z)-plane be inward spirals, i.e.

$$D \equiv \tfrac{1}{2}\theta^2 - \omega^2 - 3\gamma^2 < 0,$$

where $\theta^2 = \mathrm{def}\boldsymbol{u} \cdot \mathrm{def}\boldsymbol{u}$. In our notation, and for the postulated initial velocity field, this is equivalent to

$$\Gamma^{*2} A_R > (8\pi^3)^{-1}.$$

If we exclude from consideration vortices that suffer collapse, and use criterion (3.10) for the collapse of elongated vortices, this leads to

$$A_R < 4.$$

Thus elongated vortices whose circulation is insufficient to cause collapse are also incapable of winding material surfaces around their centres in competition with the inward advection of the strain velocity. The interfacial surface is merely distorted into an approximately sinusoidal shape with wavelength λ and amplitude equal to that of the excursions of the vortex tips from the z-axis. This amplitude increases as the aspect ratio decreases; but, even for $A_R = 4$, our numerical solutions yield, for non-collapsing vortices, an amplitude < 0.16 for which the interfacial length $< 1.2\lambda$. Thus, even for thick (non-collapsing) vortices, the maximum possible increase in diffusion rate afforded by the presence of the vortices does not exceed 20 %. Note that,

under these circumstances, any visualization method which depends on the diffusion of a scalar such as spark shadowgraphy or a diffusion-controlled reaction would fail to betray the presence of the vortices.

Figure 11 (*a–b*) describe the different trajectories of fluid particles when the vortices are weak and elongated (*a*) and when they are strong and concentrated (*b*).

3.6.2. *Results of the numerical simulations*

The initial distribution chosen for ρ in the numerical solutions of (2.2*d*) is that given by (3.15*a*, *b*) for plane strain alone. As mentioned in §3.6.1 this choice is consistent with that of the similarity solution for the initial vorticity distribution. In all cases discussed, $\nu/D = 1$.

Figure 12 shows contours of concentration and vorticity for vortices that will eventually suffer partial collapse ($\Gamma^* = 0.04$, $A_R = 11.25$, a case which falls between the two solid curves on figure 9) at a time which is about τ_c. The innermost vorticity contours already show the early result of focusing due to self-induction (both the intensity of ω at the centre and the thickness of the layer have increased slightly). The concentration-layer profile is still almost totally unaffected by the circulation. The contour on which $\rho = 0$ is displaced up and down but its thickness and profile have practically not changed since $\tau = 0$. This and all other calculated cases for which either the value of $\Gamma^* A_R$ was insufficient to collapse or at times for which collapse had not yet substantially redistributed the vorticity, exhibit the concentration contours associated with weak vortices in §3.6.1.

When most of the vorticity is advected inwards, the history of the concentration gradient layer is radically different. Figure 13 (*a–c*) describes such a case. Initially, $\Gamma^* = 0.1661$, $A_R = 11.25$, and the collapse time calculated by the model equation is $\tau_c = 1.4$. For this run the value of γ varied with τ as

$$\gamma = \gamma_0 \frac{3}{3+\tau}.$$

Thus Γ^* increases as $\frac{1}{3}(3+\tau)$ and A_R decreases as $[\frac{1}{3}(3+\tau)]^{-\frac{1}{2}}$. This variation of γ is not of great importance, since the initial value of $\Gamma^* A_R$ is sufficient to cause collapse in a short time. It was used to simulate conditions at a stagnation point in a mixing layer while it pairs. The γ variation also has the advantage of providing a better resolution for the calculations because the lengthscale for diffusion increases as $\gamma^{-\frac{1}{2}}$ as the computation proceeds.

At $\tau = 1$ the diffusion layer steepens and thickens at the midplane. At $\tau = 1.5$, when the centres of the vortices have started to shrink and rotate rapidly, the concentration profiles start to participate in the vortex circulation, and at $\rho = 2.5$, when the vortices have nearly completed their collapse, the concentration layer has rolled up into a characteristic mushroom shape. A later stage of the transformation can be viewed in figure 14 for a case for which $\Gamma^* A_R$ is almost the same as in the preceding case, but Γ^* is doubled while A_R is approximately halved, so that the collapse time is shortened by a factor of about 4. It can be noticed that most of the area occupied by the round vortices has been so effectively mixed as to yield an almost-uniform concentration. Figures 13 and 14 are strikingly similar to photographs obtained from laser-induced fluorescence patterns in a water mixing layer by Bernal (1981), and they offer support for the suggestion by Bernal that these patterns are caused by the presence of (in fact, as we saw, by the collapse of) streamwise vortices. Figure 15 shows the ratio of the mixed volume at any time to that which would result from strain alone for several cases in which γ is constant and vortices suffer collapse.

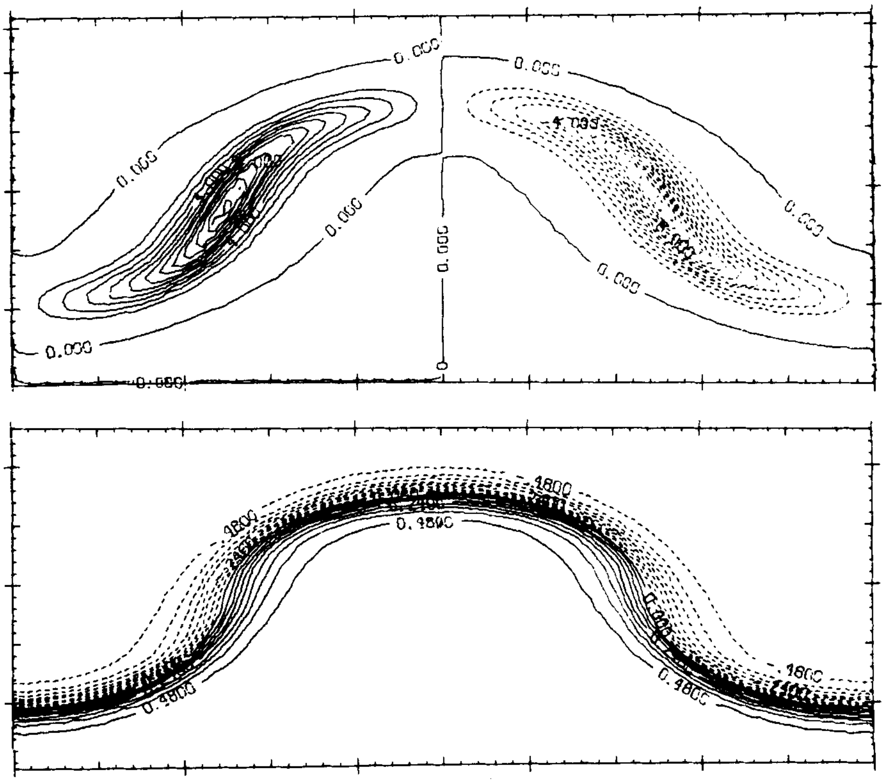

(*a*)

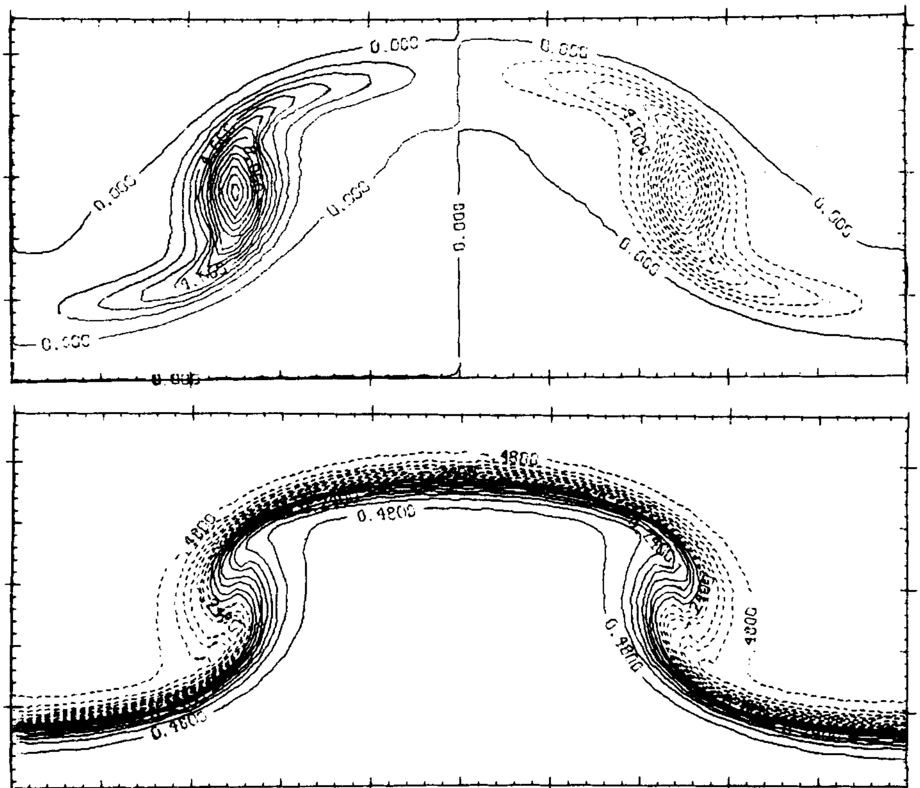

(*b*)

FIGURE 13 (*a*, *b*). For caption see facing page.

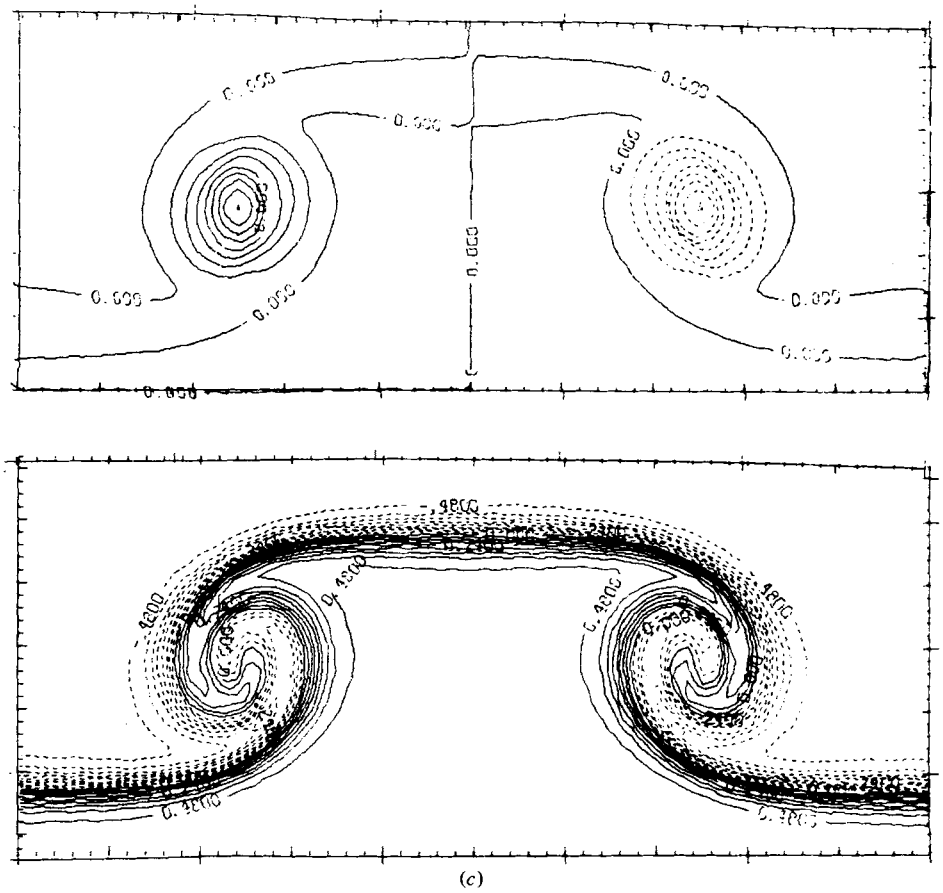

(*c*)

FIGURE 13. Vorticity and concentration contours: (*a*) $\tau = 1.0$; (*b*) 1.5; (*c*) 2.5. Vorticity-contour intervals are 1.0 (*a*, *b*) and 2.0 (*c*). $\Gamma^* = 0.166$, $A_R = 11.25$.

But the runs were clearly not long enough for the mixing rates to reach an asymptotic value. In §3.6.3 we determine how these rates depend on the flow parameters.

3.6.3 *Mixing rate after collapse*

As explained in §3.5, collapsed vortices in planar strain reach in a time of order γ^{-1} a well-defined structure, that of the axially symmetric Burgers vortex. Under many conditions it thus becomes possible to analyse the effect of the streamwise vortices on the final rate of diffusion of the scalar with the initial conditions of §3.6.2. Neu (1984*c*) and Karagozian (1982), elaborating on earlier work by Marble (1984), have examined the effect of an axially symmetric vortex in an axially symmetric strain on the diffusion of a scalar originally distributed uniformly over, say, the top half-plane $y, z > 0$. A material surface that coincides initially with the concentration discontinuity at $z = 0$ forms a double spiral around it. Diffusion of the scalar is far more rapid across this surface than along it. This allows the above authors to use the parabolic approximation discussed in Part 1. The analysis leads first to the determination of the configuration of the material surface at any time and of the strain along it, and secondly to a local solution of the diffusion operator for the concentration layer which straddles the material surface. Marble and Karagozian view the diffusion

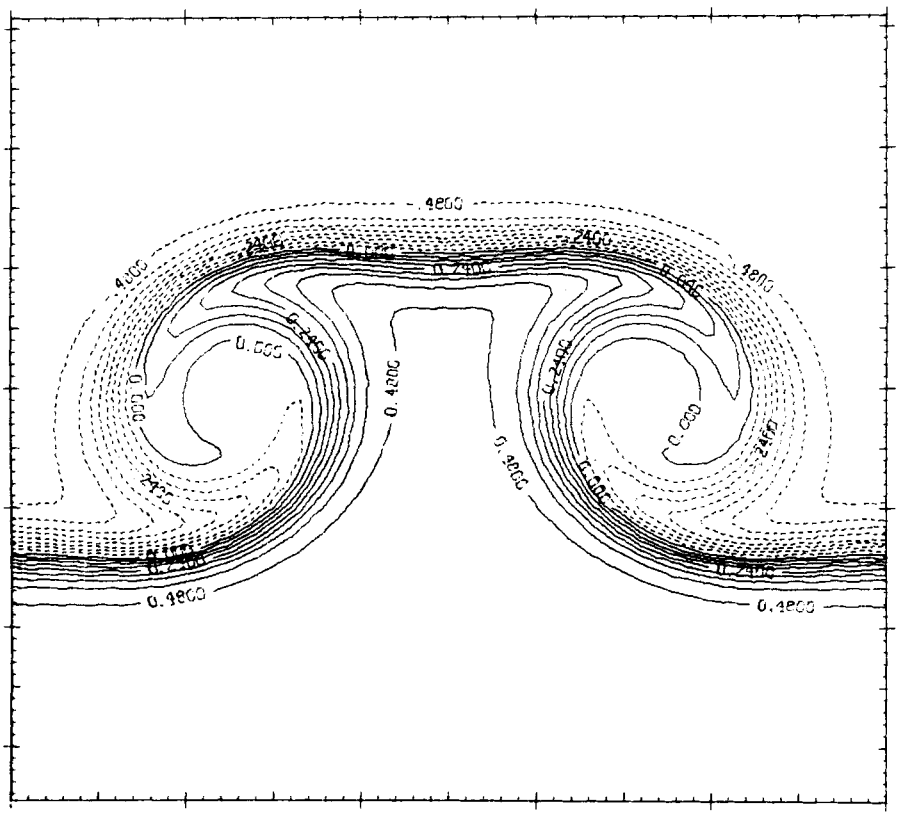

FIGURE 14. Concentration contours; $\Gamma^* = 0.64$, $A_R = 4.73$, $\tau = 3.0$. The corresponding vorticity contours are shown on figure 10.

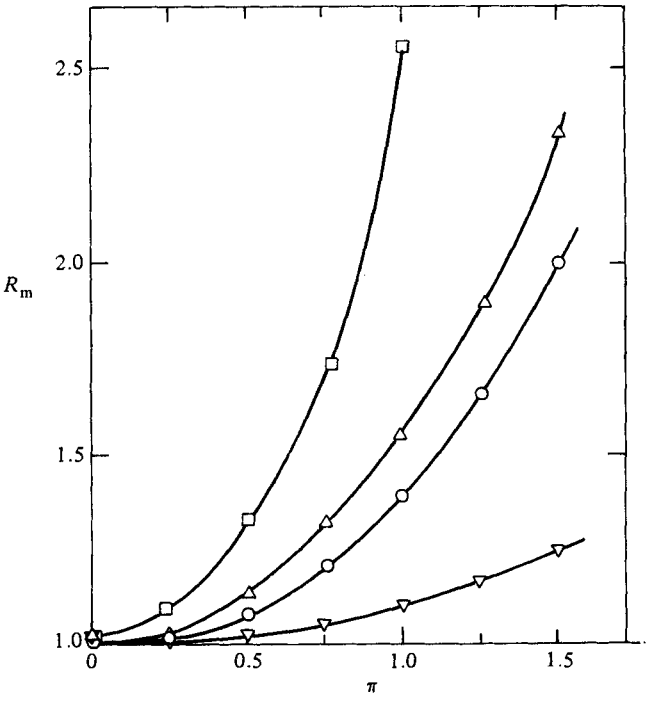

FIGURE 15. The ratio of mixed volume to that from strain alone as a function of time: ∇, $\Gamma^* = 0.16$, $A_R = 11.25$; $\bigcirc$, 0.32, 7.95; $\triangle$, 0.32, 15.87; $\square$, 0.64, 15.87.

field as made of two regions – one in which the material surface is loosely folded and the diffusion layers are distinct from each other, and the other in which the radial distance between two adjacent turns of the spiral is smaller than the diffusion thickness of the concentration layer. The latter region they consider fully mixed. Neu has verified the soundness of this point of view by providing an analysis of the mixing zone wherein the diffusion layers interfere with each other. He is thus able to provide an explicit estimate for the additional rate of creation of mixed volume, free of undetermined constants. When the material interface has reached an asymptotically stationary trace in the (y, z)-plane, which requires a time of order γ^{-1}, that estimate is

$$\frac{\mathrm{d}V_{\mathrm{m}}}{\mathrm{d}t} = 1.50 D^{\frac{1}{3}} \Gamma^{\frac{2}{3}} \mathrm{e}^{\gamma t} \tag{3.18}$$

for a unit initial length in the x-direction. Since for the strained diffusion layer of span $\frac{1}{2}\lambda$, in the absence of vorticity, the rate is

$$D\delta_D^{-1} \mathrm{e}^{\gamma t} = \left(\frac{2}{\pi}\right)^{\frac{1}{2}} \lambda \gamma^{\frac{1}{2}} D^{\frac{1}{2}} \mathrm{e}^{\gamma t},$$

the ratio of mixing rates is

$$R_{\mathrm{m}} = 1.88 \Gamma^{\frac{2}{3}} D^{-\frac{1}{6}} \lambda^{-1} \gamma^{-\frac{1}{2}}, \tag{3.19a}$$

or in terms of our parameters,

$$R_{\mathrm{m}} = 3.22 A_{\mathrm{R}}^{\frac{1}{3}} \Gamma^{*\frac{2}{3}} \left(\frac{\nu}{D}\right)^{\frac{1}{6}}. \tag{3.19b}$$

Because the region that contributes most to the mixing extends beyond the vortex radius, it is necessary, in order to make use of the above results to examine the effect of plane strain on the evolution of the material interface, given that the vorticity is distributed in a row of Burgers vortices of equal strength and alternating circulation. H. King (unpublished work) has provided the details of this analysis. In regions that for collapsed vortices satisfy the condition

$$\left(\frac{r}{\delta}\right)^2 \ll \frac{3.3}{\pi^2} A_{\mathrm{R}}^3,$$

where r is the radius from the vortex centre to a point on the material interface and δ is the vortex radius, the equation for the half of the material interface initially found on $z = 0$, $y > 0$ is

$$\theta - \tfrac{1}{2}\sin 2\theta = \frac{\Gamma}{2\pi r^2}\left[1 - \exp\left(-\frac{\gamma r^2}{r\nu}\right)\right] - \frac{\Gamma}{8\pi\nu} E_{\mathrm{i}}\left(-\frac{r^2}{4\nu}\right),$$

where

$$E_{\mathrm{i}}(-u) = -\int_u^\infty \frac{\mathrm{e}^{-u}}{u}\,\mathrm{d}u,$$

and θ is measured from the positive y-axis.

For large values of θ the term $\sin 2\theta$ can be ignored in the above expression. The effect of the other vortices can also be shown to be small under the same circumstances. The component of strain along the interface and in the (y, z)-plane, once averaged over θ, is also found to be the same as in the axially symmetric case. When the radius

at which diffusive layers begin to overlap is greater than the radius containing vorticity, i.e. when

$$\left(\frac{r^*}{\delta}\right)^2 = 2^{\frac{7}{3}}\pi^{-\frac{1}{3}}(\Gamma^* A_A^2)^{\frac{2}{3}}\left(\frac{D}{\nu}\right)^{\frac{1}{3}} \gg 1, \tag{3.20}$$

the rate of increase of mixed volume is that given by (3.18) and the ratio of mixing rates that given by (3.19). Condition (3.20) is easily satisfied for gases and generally satisfied at high Reynolds numbers. In figure 14, where the transient phase for mixing is still incomplete, the region of uniform concentration centred on the vortex is already larger than the latter.

We note from (3.19) that the increase in mixing rate due to the collapse of the vortices is only proportional to the $\frac{1}{6}$ power of the Schmidt or Prandtl number.

4. The instability of a strained uniform vortex layer

We now return to the first question raised in §2.2. To isolate the problem of the spontaneous instability of elongated vortices from that of the bulk redistribution of their vorticity, we assume that these vortices have infinite aspect ratio, i.e. that their circulation $\sigma_0 = 2V_0$ per unit length is initially uniform. They are then described by (2.6) with $\beta = 0$, a solution to the full equations of motion which was probably first given by Burgers (1948).

The discussion of §3 leads us to suspect that such layers are unstable and that Neu's criterion (3.12) might apply. Neu has in fact dealt with this problem in the same paper (Neu 1983*b*) in the context of long waves. However, we recall that the time required for collapse, which can be thought of in this context as an inverse growth rate for a perturbation, decreases as the inverse square of Γ^*. This leads us to guess that the relevant wavelengths of instability are not long next to the layer thickness and these are beyond the scope of Neu's asymptotic theory.

4.1. *Instability of infinitesimal perturbations*

We first formulate the linear or infinitesimal-perturbation version of the stability problem. Equations (2.2*a–c*) are linearized around the steady solution of the Burgers vortex layer after they are non-dimensionalized by using $\delta = (\pi\nu/2\gamma)^{\frac{1}{2}}$ as the unit of length and $V_0 = \frac{1}{2}\sigma_0$ as the unit of velocity. We then assume that the perturbation velocities are two-dimensional. Their stream function ψ is written

$$\psi = \phi(z)\exp \mathrm{i}\alpha(y - ct),$$

in terms of which the linearized vorticity equation becomes

$$(V-c)\,\phi'' - \alpha^2\phi - \phi V'' = -\frac{\mathrm{i}}{\alpha R}\left[\phi^{\mathrm{iv}} - 2\alpha^2\phi'' + \alpha^2\phi + \frac{\mathrm{d}}{\mathrm{d}z}(\phi'' - \alpha^2\phi)\right], \tag{4.1}$$

where

$$R = \frac{V_0\delta}{\nu} = V_0\left(\frac{\pi}{2\gamma\nu}\right)^{\frac{1}{2}}, \quad \alpha = k\delta = k\left(\frac{\pi\nu}{2\gamma}\right)^{\frac{1}{2}}.$$

We note that the left-hand side of (4.1) is formally identical with the inviscid approximation to the Orr–Sommerfeld equation, so that as $\alpha R \to \infty$ we expect its solution to tend to that for the unstrained layer for high Reynolds numbers. This also follows from

$$\alpha R = \frac{\pi}{4}\frac{k\phi_0}{\gamma}.$$

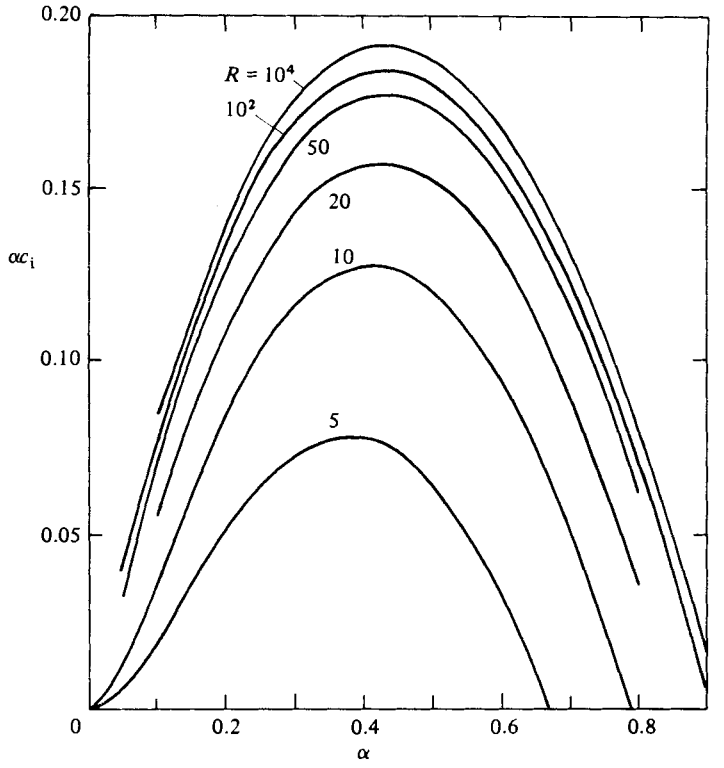

FIGURE 16. The eigenvalues of the initial instability of the Burgers vortex sheet: growth rate αc_i *vs.* wavenumber α for six Reynolds numbers.

The boundary conditions used in the solution of (4.1) are

$$\phi \to \exp(\mp \alpha z), \quad \phi'' - \alpha^2 \phi \to 0 \quad \text{as} \quad z \to \pm\infty.$$

These ensure asymptotically irrotational and bounded solutions. An efficient elaboration of the Thomas algorithm was used to find the eigenvalues and to generate eigenfunctions. Details and in particular the eigenvalues of the lowest mode for a range of values of the two parameters α and R are given in Lin (1981). Figure 16 summarizes these results in terms of the growth rate αc_i, where $c_i = -ic$ (since, in the present problem, the real part of c vanishes). A comparison of these values with those appropriate to an unstrained layer reveals that the maximum growth rate is comparable, though it occurs at a somewhat higher wavenumber in the strained than in the unstrained case. A typical value of α for the fastest-growing wave is $\alpha = 0.4$.

It is of interest to compare these results with those of Neu (1984*b*), which apply in the limit $\alpha R \to 0$. His inviscid dispersion relation is to leading order

$$\frac{\alpha_N}{\gamma} = \frac{1}{2}\left[1 + \left(\frac{\sigma_0 k}{\gamma}\right)^2\right]^{\frac{1}{2}} - \tfrac{1}{2}, \tag{4.2}$$

where the equivalence between his notation and ours is given by

$$\frac{\alpha_N}{\gamma} = 2\pi^{-1}(\alpha c_i)\, R, \quad \frac{\sigma_0 k}{\gamma} = \frac{4\alpha R}{\pi}.$$

The only range of values for which agreement between the two calculations might

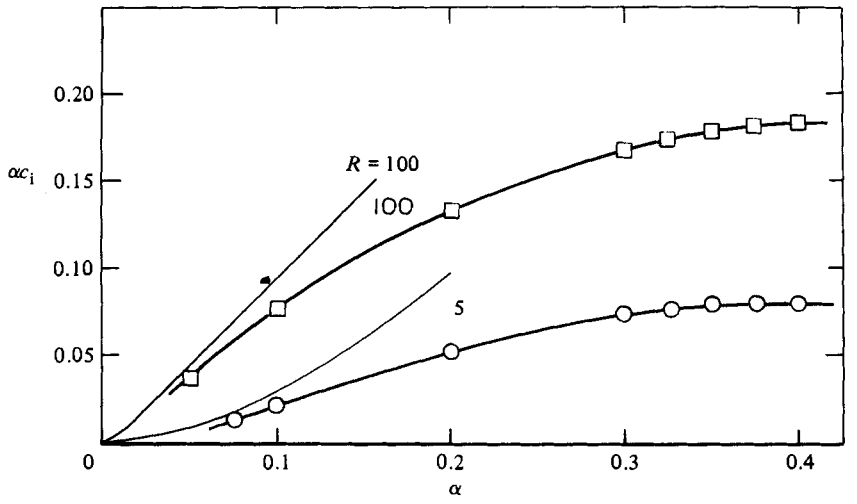

FIGURE 17. The growth rate for long waves: a comparison of Neu's inviscid asymptotic theory with the eigenvalues for the viscous layer of finite thickness.

be expected is $R \to \infty$, $\alpha \to 0$ in such a way that $\alpha R \to 0$. In fact (figure 17), for a given small value of α, the agreement improves slowly as $R \to \infty$, even though $\alpha R \propto k\sigma_0/\gamma$ becomes large. This suggests that Neu's linearized dispersion relation above requires only $k(\nu/\gamma)^{\frac{1}{2}} \ll 1$, rather than both $(k\sigma_0/\gamma)^{\frac{1}{2}}$ and $\sigma_0/(\nu\gamma)^{\frac{1}{2}} \ll 1$.

4.2. *The nonlinear evolution of the instability*

We now use numerical finite-difference solutions to follow the development of the instability beyond the infinitesimal stage. Equations (4.2) are solved as in §3 and the boundary conditions are the same, with the exception that

$$V \to \pm 1 \quad \text{as} \quad z \to \pm \infty.$$

The numerical scheme is almost the same as that discussed in §3.2 (see Lin 1981). For initial conditions, we use the superposition of the error-function profile and eigenfunctions of (4.1) with a small amplitude. The calculation of the growth rate of the perturbation energy over the first few time steps serves as a check of the accuracy of the numerical procedure. This growth rate is found to agree with the predictions of linear theory with a maximum error less than 2%.

Two cases were run for which the initial wavenumber $\alpha = k\delta$ is approximately that for maximum initial growth according to figure 15. They correspond to $R = 50$ and $R = 20$.

Figures 18(*a–c*) show the evolution of the vorticity contours for $\tau = 1.0$, 2.0 and 4.0 for $R = 50$. The initial evolution is quite similar to that of the unstrained case at the same Reynolds number and corresponding times. This is expected from the results of the linear analysis. But at $\tau = 4.0$ we notice two consequences of the presence of axial strain: the first is that the maximum value of the vorticity has risen at the centre (from 14.8 at $\tau = 0$ to about 20 at $\tau = 4$). The second is that the vorticity has completely left the braids. The evolution of the rolled-up vortex is far from over at the end of the calculation. The asymptotic state for large values of τ is discussed in §4.3.

For $R = 20$ (figures 19*a–c*), roll-up is noticeably slower, but the intensification and

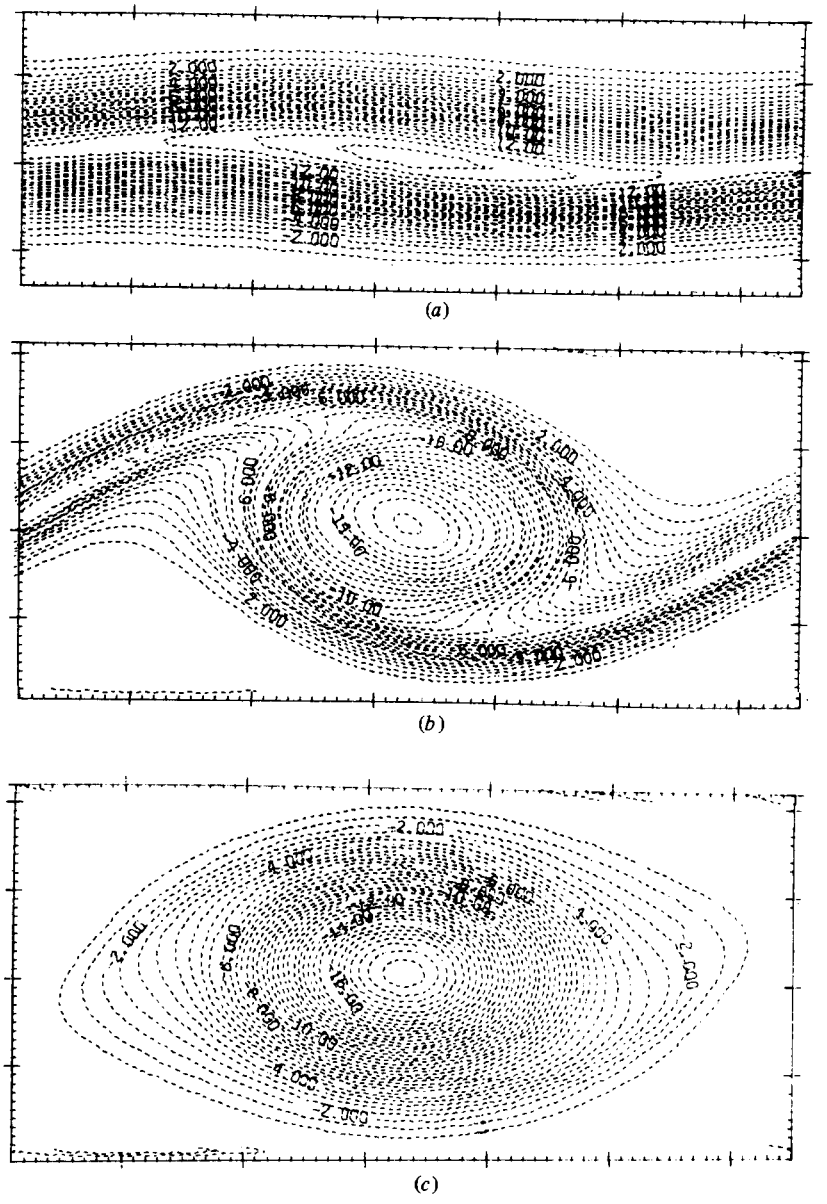

FIGURE 18. Instability of the Burgers vortex sheet according to a nonlinear numerical solution with one initial eigenfunction. Vorticity contours; $R = 50$, $\alpha = 0.40$: (*a*) $\tau = 1.0$; (*b*) 2.0; (*c*) 4.0.

shrinking of the vortex by the imposed strain is faster. At $\tau = 5.0$ the maximum vorticity already exceeds the value 30.

In the next two cases the initial conditions are the sum of wavenumber α_1 and its subharmonic with wavenumber $\alpha_2 = \frac{1}{2}\alpha_1$. The amplitude of the subharmonic is half that of the fundamental. The phase ϕ (see part 1, §4.3.2) is 0. The wavelength used as lengthscale is $\lambda_1 = 2\pi\delta\alpha^{-1}$. The gridlength is 2λ non-dimensional units.

For $R = 20$ (figure 20*a–d*) the roll-up occurs as in the previous case at $\tau = 2$. The vortices have only rotated around each other by a very small angle and their spacing

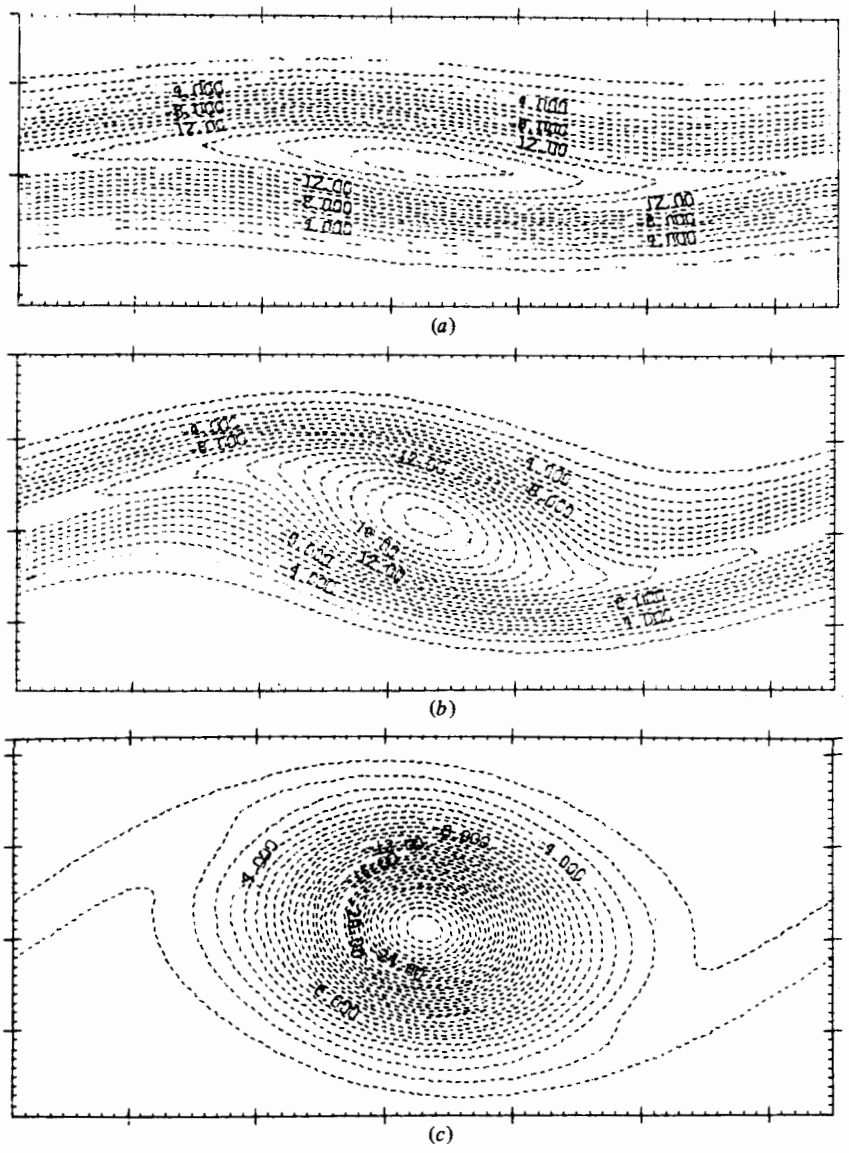

FIGURE 19. Instability of the Burgers vortex sheet (continued). One initial eigenfunction; $R = 20$, $\alpha = 0.425$. Vorticity contours: (*a*) $\tau = 1.0$; (*b*) 2.0; (*c*) 4.0.

has slightly decreased. At $\tau = 3$ the rotation is apparent and the vortices are approaching each other more rapidly. At $\tau = 4$ they have coalesced and shrunk. The concentration contours are shown on figure 20(*d*) for $\tau = 3.0$ ($\nu/D = 1$). The figure shows that mixing is complete within the individual vortices before pairing and that the strong concentration gradients where mixing takes place are external to the intense pairing vortices (see discussion of §3.6.3). For $R = 5$ figure 21, which gives the vorticity contours at $\tau = 4.0$, shows that the vortices have almost reached their equilibrium thickness but that they are distorted. The effect of the subharmonic is almost imperceptible. At $\tau = 8$ the situation is not materially altered: the two

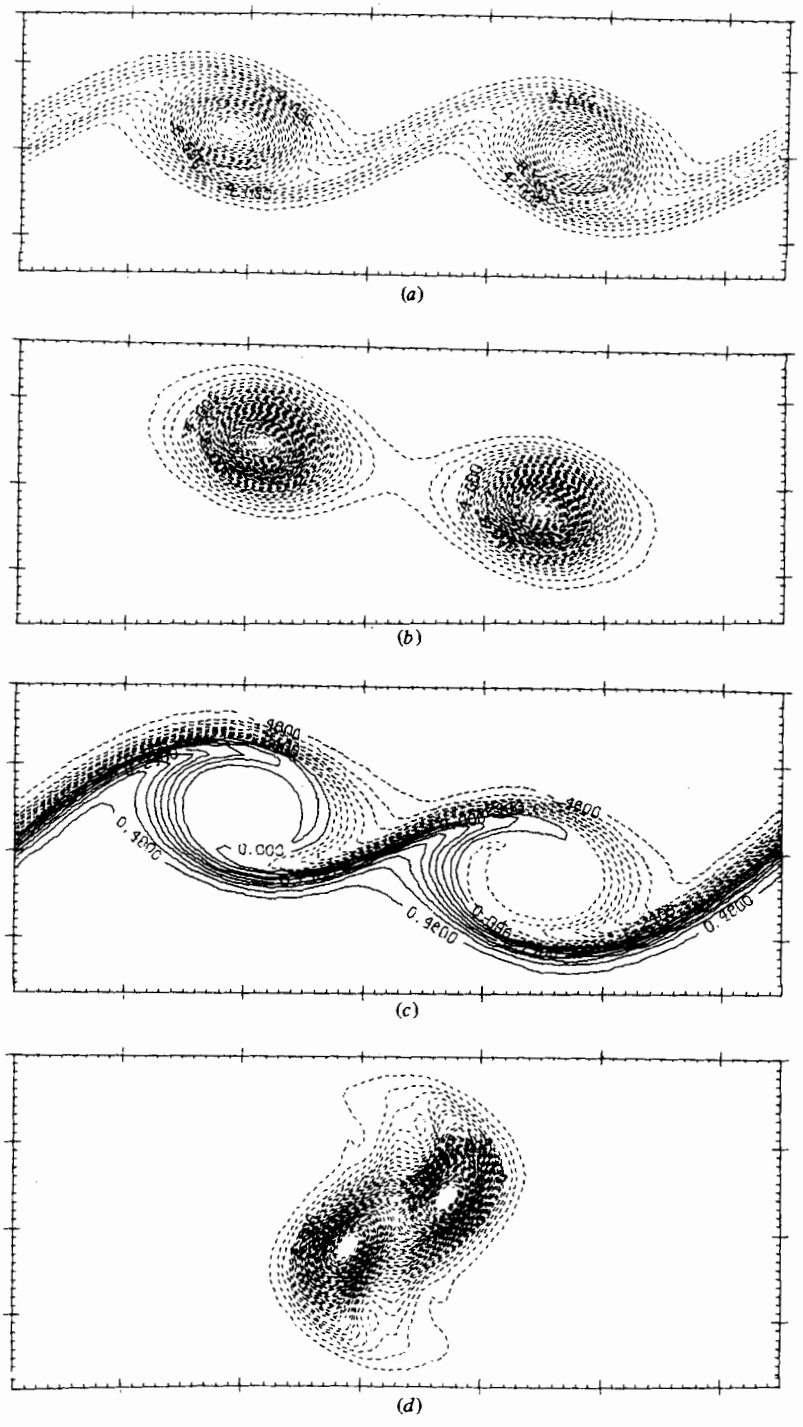

FIGURE 20. Instability (continued). Two initial eigenfunctions: $R = 20$, $\alpha_1 = 0.425$, $\alpha_2 = 0.2125$. Vorticity contours: (*a*) $\tau = 2.0$; (*b*) 3.0; (*d*) 4.0. Concentration contours: (*c*) $\tau = 3.0$.

vortices have not moved much closer together; they still lie on the y-axis and their maximum vorticity has nearly reached a constant value, approximately three times the initial maximum value. Thus in this case pairing seems to be in doubt.

4.3. *Discussion*

After the perturbations have grown beyond the linear range, the vorticity, which was initially uniform along y, tends to be concentrated into finite vortices. The flow is thus reminiscent of that discussed in §3. Yet there are important differences which lead to a qualitatively different outcome. The aspect ratio defined in §3 is now inversely proportional to α. Since the value of this parameter tends to be narrowly confined by the selectivity of the maximum initial growth rate, it can for our purposes be assumed fixed. The circulation of all neighbouring vortices now has the same sign, where it had alternating signs in §3. A consequence of the present arrangement is that an alternate perturbation of the height of the vortices (which may be caused by a first subharmonic) now leads to instability and pairing.

It is helpful to relate the parameters used in the discussion of the previous section with those that arise naturally in the present context. If we retain the definition of aspect ratio as

$$A_{\mathrm{R}} = \lambda/4\delta,$$

and note that if $\sigma_0 = 2V_0$ is the uniform strength of the initial Burgers sheet then $\Gamma_{\mathrm{r}} = \sigma_0 \lambda$ is the circulation for each vortex, then

$$R = (\tfrac{1}{2}\pi)^{\frac{1}{2}} N = \pi \Gamma_{\mathrm{r}}^* A_{\mathrm{R}}, \quad \alpha R = \tfrac{1}{2}\pi^2 \Gamma_{\mathrm{r}}^*, \quad \alpha = \tfrac{1}{2}\pi A_{\mathrm{R}}^{-1},$$

where $N = \sigma_0/2(\nu\gamma)^{\frac{1}{2}}$.

It should also be noted that the non-dimensional time used in the calculations is the one that occurs naturally in the study of linear stability, i.e. $\tau = tV_0/\lambda$. This time is related to $t\gamma$, the non-dimensional time in our study of the collapse of vortices of finite span in §3 by

$$\frac{V_0 t}{\lambda_1} \equiv \tau = (\pi^{-2}\alpha R)\,\gamma t. \tag{4.3}$$

4.3.1. *Roll-up*

In roll-up, first the interaction between the vorticity and the strain associated with that vorticity alters the strain–diffusion balance implied in the base state by redistributing the vorticity of a layer into thicker and separated vortices. Then the external strain forces a strain–diffusion balance for the new configuration of vorticity by stretching the vortices, which become more intense and acquire a smaller cross-section. These two physical processes are not independent: the imposed strain tends to inhibit roll-up, and, after roll-up occurs, the strain created by the row of vortices may be a major, though decreasing, perturbation of the imposed plane strain.

The two stages of the evolution are most distinct and therefore easier to identify when the imposed strain is comparatively weak, i.e. when R is large, because their timescales are then quite different: the roll-up timescale is simply λ/V_0 as in the unstretched case, while the stretching timescale is $1/\gamma$, so that the ratio of the time required to achieve a final strain–diffusion balance (i.e. stretching time) to the time required to upset the initial one (roll-up time) is, according to (3.3), about $\pi^{-2}\alpha R$. On the other hand, when the Reynolds number of the initial vorticity layer approaches the critical value for instability (which has not been determined precisely but which is bounded below by $(\frac{1}{2}\pi)^{\frac{1}{2}}$ and which, according to figure 16, is substantially

less than 5), roll-up and stretching proceed apace and their common timescale is about $1/\gamma$.

The flows shown in figures 18 and 19 at Reynolds numbers of 50 and 20 have not reached their asymptotic state by the end of the calculation. For larger times stretching takes place while the rolled-up vortices remain under each other's strong influence – thus the strain in the (y, z)-plane caused by mutual induction is still large compared with the imposed strain in the (z, x)-plane. To gain an idea of the relative intensity of these two types of strain at the vortex centres, we assume that the other vortices are concentrated at points. We thus estimate

$$\gamma_{\mathrm{v}} = \pi V_0/2\lambda,$$

or in terms of the instability parameters

$$\gamma_{\mathrm{v}} = \alpha R/2\pi,$$

where γ_{v} is the strain caused by the row of vortices. This strain has major axes along 45° lines at the centre of each vortex. We see that for large values of R each vortex will remain subjected to a large strain in the (y, z)-plane, negative along one direction inclined to the y-axis and positive along another, while it is also being stretched along its own axis. We may therefore wonder whether the asymptotic state is the same as that discussed in §3. Here, we are helped by the fact that, if we omit viscous diffusion, the situation is substantially that treated exactly by Neu (1984*a*). Our high-Reynolds-number examples correspond to the case of three-dimensional strain, for which, in his notation, $(\gamma-\gamma')/\omega \ll 1$. Neu shows that if the original strain in our (y, z)-plane is not such as to extrude the vortices into ever-lengthening filaments (which is excluded by the conditions that lead to the roll-up), the vortices slowly evolve so that their decreasing cross-section tends to a fixed shape which differs only slightly from a circular one. Diffusion will, of course, stop the vortex cross-section from shrinking when its dimension is about $(\nu/\gamma)^{\frac{1}{2}}$. The ratio r'_ω of maximum vorticity after roll-up and stretching are completed to that before roll-up is essentially fixed since the length of the vorticity layer which rolls up is closely proportional to its thickness (i.e. the value of α for the largest growth rate is almost independent of Reynolds number and ≈ 0.4, see figure 16). Thus

$$r'_\omega \approx \pi(2x \times 4)^{-1} \approx 4.$$

To summarize, for any Reynolds number the asymptotic state is an approximation to the Burgers axially symmetric vortex as it was for the collapse described in §3.

4.3.2. *Pairing*

When a row of unstrained vortices with identical circulation is perturbed so that they are displaced alternately from their initial location, neighbouring vortices rotate around each other. They will also coalesce if the ratio of their radius to their spacing is sufficiently large. In that case, the field induced by the vortices themselves gives rise both to a component of velocity that causes a rotation of the two vortices around their common centre and to an inward component along the line of centres.

If strain is imposed as in our model, the vector sum of the velocity induced by one displaced vortex on the other and of the inward strain velocity includes a component in the direction of the centre of symmetry for the two vortices. As a result such vortices should approach each other and collide or coalesce, no matter how small the ratio of their radius to their initial spacing, and provided only that they are initially perturbed in alternating fashion.

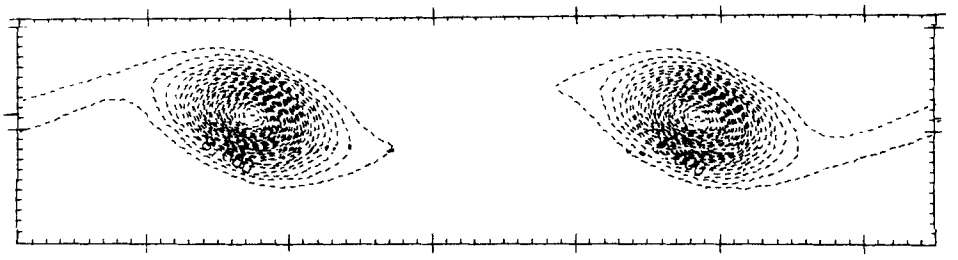

FIGURE 21. Instability (continued). Two initial eigenfunctions:
$R = 5$, $\alpha_1 = 0.375$, $\alpha_2 = 0.1875$, $\tau = 4.0$.

A simple calculation suitable for highly concentrated vortices shows that the initial relative collision velocity is $2\Gamma_r A_0/\pi\lambda^2$, so that the coalescence time is of order

$$\tilde{\tau} = \tfrac{1}{2}(\lambda/A_0),$$

where A_0 is the amplitude of the normal displacement of the vortices. In this expression, if A_0 is the result of a naturally occurring subharmonic perturbation (instead of being imposed) its value will depend inversely on the strain rate γ. Thus we should expect that the coalescence time would increase as R decreases. This is borne out by the calculations for $R = 50$ and $R = 20$. For the case $R = 5$ the numerical solutions indicate that the subharmonic perturbation is so small that its effect is practically undetectable. According to figure 17, the initial growth rate of this perturbation (with $\alpha = 0.1875$) is positive, though small. But by the time the sheet has rolled up into the concentrated vortices of figure 21 the numerical evidence is that the subharmonic has decayed to negligible amplitude. The reason for this decay is not yet clear.

Whenever pairing occurs, the asymptotic value of the maximum vorticity should nearly double after the new equilibrium is reached between stretching and diffusion.

5. Stretched vortices in the mixing layer

Part 1 showed that the evolution of a two-dimensional mixing layer consists in the redistribution of the original layer vorticity into spanwise vortices of increasing circulation and spacing. These cause a two-dimensional strain field whose lengthscale also increases in time (for the T-layer) or downstream (for the S-layer). Part 2 showed that, while a mixing layer readily acquires three-dimensional components of motion and vorticity components in planes perpendicular to the span, the basic features of the two-dimensional flow studied in Part 1 survive with little change so that the largest-scale strain is found in the (x, z)-plane.

As was remarked in §1, the model of the environment that we have chosen to study the evolution of streamwise vorticity selectively focuses on one of these features, the clear tendency of the base flow to stretch the streamwise vortices on the average. The focus is achieved by ignoring several other interactions between streamwise and spanwise vorticity. Thus when streamwise vortices are rolled into large spanwise vortex structures, the principal axis of positive strain of the primary flow does not in general coincide with the direction of the streamwise vorticity, so that this vector tends to be rotated and in the process probably experiences temporarily negative strain along it. In addition, concentrated streamwise vortices are sure to alter the local distribution of spanwise vorticity. We are not prepared to evaluate here the

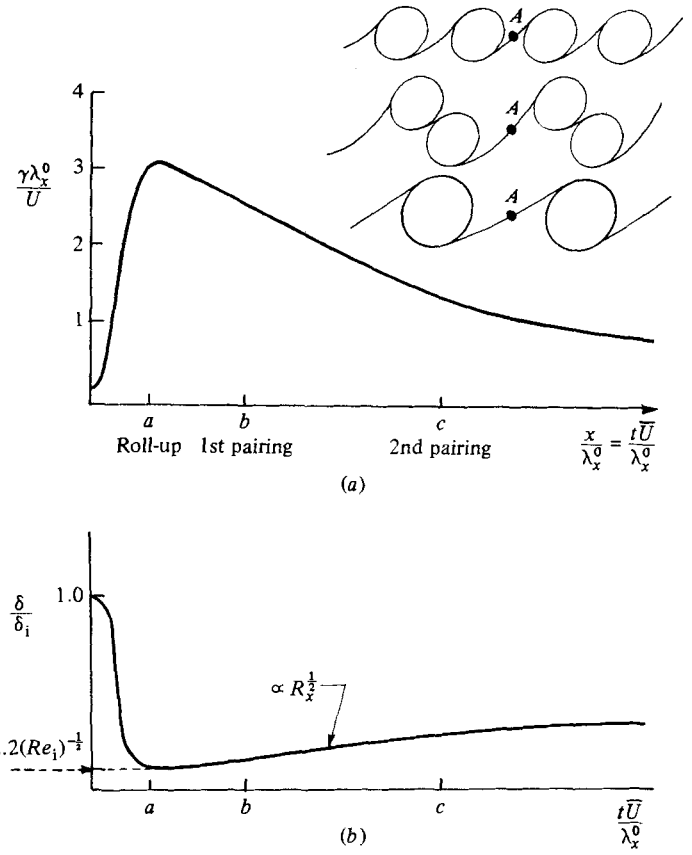

FIGURE 22. Sketch of the streamwise variation of the strain γ (*a*) and of strain-controlled diffusion-layer thickness δ (*b*) in the mixing layer near a surviving stagnation point A between spanwise vortices.

consequences of these complications. But we wish to infer from the results of the model study the probable behaviour of streamwise vorticity in those simpler parts of the mixing layer where the model is relevant.

The evolution of strain along an initial material interface near a surviving stagnation point A as it is followed downstream, starting with the origin of the layer, is sketched on figure 22 (*a*). The strain has a low initial value and rises to approximately 3 at the end of the roll-up ($\gamma t \approx 2$, point *a*). It then decreases as a result of pairing, each pairing decreasing it by a factor of 2. Correspondingly, the thickness of the vorticity layer first decreases rapidly. One finds for instance that if the initial wavelength of the two-dimensional instability that leads to the roll-up of spanwise vorticity is $(\lambda_x)^0 = 15\delta_i$, where δ_i is the initial-layer thickness, when $\gamma \approx 3U/(\lambda_x)^0$ (i.e. towards the end of roll-up) then

$$\frac{\delta}{\delta_i} \approx \left(2.8\frac{U\delta_i}{\nu}\right)^{\frac{1}{2}}. \tag{5.1}$$

The evolution of δ is sketched on figure 22 (*b*). Generally δ increases by a factor of $2^{\frac{1}{2}}$ through each successive pairing. The aspect ratio of streamwise vortices, i.e. (vortex spacing)/2δ, is determined by the ratio $(\lambda_x)^0/\lambda_y$ (which in the terminology of

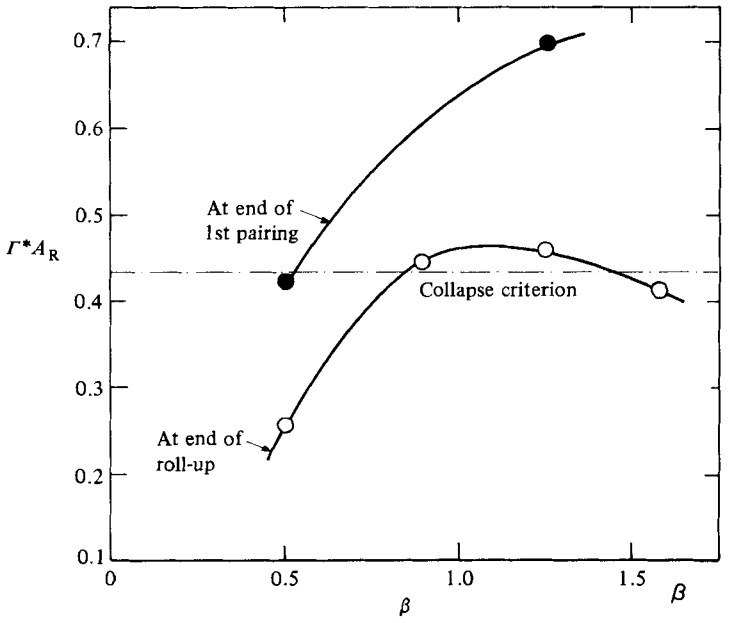

FIGURE 23. The variation of the primary collapse-controlling parameter $\Gamma^* A_R$ as a function of spanwise wavenumber β (from the calculations of Part 2).

Part 2 is β) and by (2.6c). Thus we find that at the end of roll-up, using approximation (5.1),

$$A_R = 1.34\beta^{-1}\left(\frac{U\delta_i}{\nu}\right)^{\frac{1}{2}}. \tag{5.2}$$

For a fixed value of β, A_R would decrease by a factor of $2^{\frac{1}{2}}$ as a result of pairing.

5.1. *The occurrence of the collapse of streamwise vortices in the mixing layer*

We wish to predict approximately how far downstream streamwise vortices in the neighbourhood of stagnation points will collapse (and be visible by concentration-gradient-sensitive optical techniques). We thus need to evaluate both where the conditions for collapse are met and how much later collapse is completed.

We recall from (3.12) that an approximate criterion for substantially complete collapse with $\sigma_c/\sigma_0 = 0.3$ is

$$\Gamma^* A_R > 0.43.$$

If we define $\Gamma_{II} = \Gamma(U(\lambda_x)^0)^{-1}$ and $\gamma_I = \gamma(\lambda_x)_0 U^{-1}$, from (5.2), we find that

$$\Gamma^* A_R = 1.34\beta\gamma_I^{-1}\left(\frac{U\delta_i}{\nu}\right)^{\frac{1}{2}}\Gamma_{II} \tag{5.3}$$

at the end of the roll-up. Each pairing increases this value roughly by a factor of $2^{\frac{1}{2}}$. In (5.3) we assign the typical value $\gamma_I = 3$ from Part 1. Now typical values of the circulation around streamwise vortices are not yet known dependably. In particular, the influence of initial conditions and of initial Reynolds number are still matters of speculation. Two estimates of Γ near the centre of the braids (i.e. about halfway between spanwise vortices) are available. The first is the direct result of the numerical

calculations reported in Part 2. It gives Γ_{II} at a fixed value of initial Reynolds number $Re_i = 50$ for a range of values of spanwise spacing β. Since in those calculations Γ depends almost linearly on the amplitude of the assumed initial perturbations, a choice of initial amplitude was made to yield a value of spanwise velocity amplitude typical of experiments. The resulting values of Γ_{II} will next be used to evaluate $\Gamma^* A_R$ from (5.3). The second estimate of Γ is given by Jimenez (1983). It is an inference from experimental observations which suggests substantially higher values of circulation. It will not be used, but it would lead to the prediction of earlier collapse.

Figure 23 is the resulting plot of $\Gamma^* A_R$ as a function of β for $Re_i = U\delta_i/\nu = 50$. The approximate collapse condition is shown as a horizontal line. We see that for $\beta > 1.0$ the condition is met at the end of roll-up and easily exceeded at the end of the first pairing. At higher values of initial Reynolds number, according to (3.3), the value of $\Gamma^* A_R$ would be correspondingly higher. We note that collapse is to be expected even at very modest initial Reynolds numbers. The assumed circulation associated with the streamwise vortices amounts to about $\frac{1}{10}$ that of the spanwise vortices creating the strain at roll-up.

The time required for collapse is approximated, from (3.8), as

$$\gamma t_c = \tau_c \approx 0.04 \Gamma^{*-2},$$

which is also

$$\tau_c \approx 0.04 \gamma_I^2 \Gamma_{II}^{-2} \beta^{-4}.$$

It is thus nearly independent of initial layer Reynolds nunber, but much smaller for short spanwise wavelengths than for long ones. Using the same values of Γ_{II}, we find that at the end of the roll-up the collapse time is about 10 units for $\beta = 1.25$ and $\beta = 1.59$, and much longer for $\beta = 0.5$. At the end of first pairing this time has dropped to about 1 unit for $\beta = 1.25$ and about 20 units for $\beta = 0.5$. Since the time required for a second pairing is about 5 units, we conclude that collapse is not likely to be achieved at roll-up, but should be completed shortly after a first pairing for spanwise wavelengths equal to or somewhat shorter than the streamwise wavelength of the initial instability.

5.2. *The breakdown of a vortex by local shear instability*

When the counter-rotating vortices have a sufficiently large aspect ratio, it is possible, as was noted in connection with figures 7 and 8, for the shear instability of these flattened vortices to give rise to smaller vortices whose spacing is about 15δ, while the vortex begins to collapse. We found in §4.3 that for sufficiently high values of Reynolds number the streamwise vorticity roll-up time associated with this instability is about $15\pi/R$, while according to §3.4, for highly elongated vortices, the collapse time is roughly $0.04\Gamma^{*-2}$. The ratio of roll-up time τ_R to collapse time is then found to be $\tau_R/\tau_c \approx 190 \Gamma^* A_R^{-1}$.

This ratio increases with the strength of the vortices, but decreases as the aspect ratio (i.e. the initial layer Reynolds number) is raised. For the case of figure 7, $\tau_R/\tau_c \approx 1.0$, while for that of figure 8, $\tau_R/\tau_c = 0.7$. In general, since a typical value of τ_R is $\approx 20(U\delta_i/\nu)^{-\frac{1}{2}}$, the small-scale spanwise segregation of streamwise vorticity of the same sign should be observed early in the development of the layer (i.e. simultaneously with the original roll-up of the spanwise vorticity) for an initial Reynolds number Re_i of about 400 or more. In view of (5.1) these smaller vortices would have a temporary spacing of about $40(U\delta_i/\nu)^{-\frac{1}{2}}\delta_i$, and they would probably

appear in plan views of mixing layers by causing streamwise streaks of spanwise concentration gradients with half this spacing.

5.3. *Collapse and the mixing transition*

Konrad (1977) and Breidenthal (1981) have measured the rate of generation of reaction product caused in a mixing layer by a diffusion-limited reaction between substances segregated upstream of the layer origin. Breidenthal's experiment was in water, Konrad's in gas mixtures, so that the Schmidt number differed by about 10^3. They both observed a rapid increase in the rate of reaction around a streamwise station whose location varied primarily with the initial layer Reynolds number. This increase they called the mixing transition.

In view of the discussion of §3.6, it is tempting to associate this phenomenon with the occurrence of the collapse of streamwise vortices. Indeed Breidenthal's observations of the location of this mixing transition seem to be consistent with the predictions of §5.1. The ratio of the rate of generation of reaction product after collapse to that before should be the same at the ratio of mixing rates (3.19), so that we would expect that ratio to depend on $(\nu/D)^{\frac{1}{6}}$, i.e. to differ by a factor of about 3 in experiments involving water and gases. According to Breidenthal, they differ by a factor of almost 6. Thus the collapse of streamwise vorticity according to theory and the mixing transition according to experiments occur at about the same stage of the mixing-layer evolution and both result in a striking loss in the ability of the molecular diffusion coefficient to control mixing rates. But, according to the experiments, this loss is even more complete than if it were due only to collapse, as though additional small scales of motion appear soon afterwards and cause even more complete mixing. However, the discrepancy noted above may not be meaningful, because the methods used to measure concentration in the two experiments were very different and possibly subject to experimental errors. In any case, it seems probable that at least the outset of the mixing transition is caused by the collapse or concentration of streamwise vortices.

6. Conclusions

The effect of two-dimensional spatially uniform strain on vorticity aligned with the positive strain direction is both striking and simple: the strain tends to generate vorticity layers with thickness $(\nu/\gamma)^{\frac{1}{2}}$, but wherever the strength of such layers is substantially larger than $2(\nu\gamma)^{\frac{1}{2}}$ its vorticity is caused by self-induction to be concentrated into well-segregated round vortices whose radius is asymptotically also $(\nu/\gamma)^{\frac{1}{2}}$. In a layer where the sign of the vorticity alternates (in the direction along which strain is absent), each portion of the layer that contains vorticity of a given sign eventually contributes that vorticity to a single vortex. This may occur in a single stage if the initial layer thickness is not excessively small next to the spanwise extent of vorticity of a given sign or, otherwise, in a succession of stages involving local roll-up and pairing. The transformation from a continuous layer to isolated vortices of the same thickness causes vorticity to be intensified by a factor which is proportional to $\nu^{-\frac{1}{2}}$. The structure of the vortices becomes closely that of an axially symmetric vortex in an axially symmetric strain. The time required for completing the transition between a strained layer and a row of vortices is approximately proportional to the first power of the strain, the fourth power of the width of the fragment of the layer collapsing as a whole and inversely proportional to the second power of its circulation.

The effect of the vorticity on the diffusion of a scalar is slight until the layer has collapsed, but substantial afterwards. It can be calculated after collapse for any Schmidt and Reynolds numbers.

In a mixing layer the strained vortices have a radius whose ratio to the average dimension d of the layer (say, the diameter of the spanwise vortices) is of the order of $(dU/\nu)^{-\frac{1}{2}}$. These structures thus have a size associated with the Taylor microscale. The study presented here and the work of Neu (1984*a*, *b*) suggest that these compact and sturdy vortices are dynamically far more plausible structures on that scale than strained layers, whose existence at high Reynolds numbers seems doomed to rapid collapse in plane strain.

Our model environment for streamwise vorticity excludes several important and realistic features found in a real mixing layer. Among these are the existence of large oscillations in the component of strain along the vorticity and the presence of extensive, though generally more dilute, spanwise vorticity with which the streamwise vortices interact.

This work has been supported by the U.S. Office of Naval Research under Contract N.R. 062–665.

REFERENCES

BRACHET, M. E. & ORSZAG, S. 1982 Secondary instability of free shear layer flows. Submitted to *J. Fluid Mech.*

BERNAL, L. P. 1981 The coherent structure in turbulent mixing layers. II. Secondary streamwise vortex structure. Ph.D. thesis, Calif. Inst. Tech.

BREIDENTHAL, R. 1981 Structure in turbulent mixing layers and wakes using a chemical reaction. *J. Fluid Mech.* **109**, 1.

BURGERS, J. M. 1948 A mathematical model illustrating the theory of turbulence. *Adv. Appl. Mech.* **1**, 171.

CAIN, A. B., REYNOLDS, W. C. & FERZIGER, J. H. 1981 A three-dimensional simulation of transition and early turbulence in a time-developing mixing layer. *Stanford Univ. Dept Mech. Engng Rep.* TF-14.

CORCOS, G. M. & LIN, S. J. 1984 The mixing layer: deterministic models of a turbulent flow. Part 2. The origin of the three-dimensional motion. *J. Fluid Mech.* **139**, 67.

CORCOS, G. M. & SHERMAN, F. S. 1984 The mixing layer: deterministic models of a turbulent flow. Part 1. Introduction and the two-dimensional flow. *J. Fluid Mech.* **139**, 29.

COUËT, B. & LEONARD, A. 1980 Mixing layer simulation by an improved three-dimensional vortex-in-cell algorithm. In *Proc. 7th Intl Conf. on Numerical Methods in Fluid Dynamics, Stanford–Ames.*

JIMENEZ, J. 1983 A spanwise structure in the plane shear layer. *J. Fluid Mech.* **132**, 319–336.

KARAGOZIAN, A. 1982 An analytical study of diffusion flames in vortex structures. Ph.D. thesis, Calif. Inst. Tech. Kármán Lab. of Fluid Mech. and Jet Propulsion.

KONRAD, D. H. 1977 An experimental investigation of mixing in two-dimensional turbulent shear flows with applications to diffusion-limited chemical reactions. Ph.D. thesis, Calif. Inst. Tech. (also *Project Squid Tech. Rep.* CIT-8-PU, Dec. 1976).

LAMB, H. 1932 *Hydrodynamics*, p. 242. Dover.

LIN, S. J. 1981 The evolution of streamwise vorticity in the free shear layer. Ph.D. thesis, Univ. Calif., Berkeley, Mech. Engng Dept (also *Rep. ONR Contract* NR-062-665, 1981).

MARBLE, F. E. 1984 Growth of a diffusion flame in the field of a vortex. In *Advances in Aerospace Science* (ed. C. Casci). Plenum.

NEU, J. 1984*a* The dynamics of a columnar vortex in an imposed strain. Submitted to *Phys. Fluids.*

NEU, J. 1984*b* The dynamics of stretched vortices. *J. Fluid Mech.* (to be published).

NEU, J. 1984*c* The evolution of diffusion flames convected by vortices. Submitted to *J. Fluid Mech.*

RILEY, J. J. & METCALFE, R. W. 1980 Direct numerical simulation of a perturbed turbulent mixing layer. *AIAA 18th Aerospace Sci. Meeting, Pasadena: Reprint AIAA* 079-027C.

PATNAIK, P. C., SHERMAN, F. S. & CORCOS, G. M. 1976 A numerical solution of Kelvin–Helmholtz waves of finite amplitude. *J. Fluid Mech.* **73**, 215.

SHERMAN, F. S. 1979 User's guide to program KHINT. *Univ. Calif. Rep., Dept Mech. Engng.*